University of Stavanger

FACULTY OF SCIENCE AND TECHNOLOGY

MASTER'S THESIS

Study Program/ Specialization:	Spring semester, 2021
Marine and Offshore Technology	**Open / ~~Confidential~~**

Author: **Xu Yang**

Supervisor: **Prof. Yihan Xing**

Title of master's thesis:

Modelling of a Remotely Operated Vehicle and Tuning for Its Robust and Optimal Dynamic Positioning Control

Credits (ECTS): 30

Key words: remotely operated vehicle, Dynamic Positioning , PID control, dynamic model, Simulink modelling,	Number of Pages: 64 **Stavanger, June, 2021**

Abstract

A tuning approach for the robust and optimal dynamic positioning control of BlueROV2 subjected to currents with varying speeds and headings is presented. A 2D planar dynamic model of BlueROV2 is developed in Matlab/Simulink and used for the study. The surge, sway and yaw motions are controlled by individual PID controllers. An extensive sensitivity study is carried out on a total of nine cases with different current speeds, current headings and measurement noise levels. The results show that the tuning of a model solely using step responses from a linearized model might not produce optimal results. Further it is important to verify the system responses in time domain after tuning. Finally, it is observed that re-tuning the controllers for each simulation case generally leads to better performance. However, it is also shown that the base case controller gains are sufficiently robust and lead to good performances for the other simulation cases.

Keywords: ROV, Simulink modelling, Dynamic positioning, PID control and tuning

Table of contents

List of figures

List of tables

Chapter 1 Introduction and Background

The work of this master thesis mainly contains two parts. One is to build up a proper mathematic dynamic model for a remotely operated vehicle (ROV). The other one is to tune and get a robust and optimal dynamic positioning control for this ROV.

This chapter will briefly introduce the concepts of unmanned underwater vehicle (especially ROV) and dynamic positioning in order to make the following work intelligible and meanwhile explain the motivation of this thesis. Objectives and approach are specified then to provide a clear direction of work. Outline of the thesis report will be presented at the end of this chapter.

1.1. Unmanned Underwater Vehicle

An unmanned underwater vehicle (UUV) is often used where the mission underwater requires no operators inside the vehicle, or the task is too heavy or dangerous for operators. Since there has been a general increase in interest in the exploration and study of ocean and the exploitation of marine resources, UUVs are commonly applied in a wide range of underwater missions in many industries such as aquaculture, defense, subsea oil and gas, and scientific research. UUVs can be generally classified as remotely operated vehicles (ROVs) and autonomous underwater vehicles (AUVs). A ROV is usually controlled by an operator on the ship or on shore via a tether and are used for a wide range of operations from inspection to intervention work. AUVs on the other hand operate independently underwater for longer periods of time and are normally utilised for inspection work.

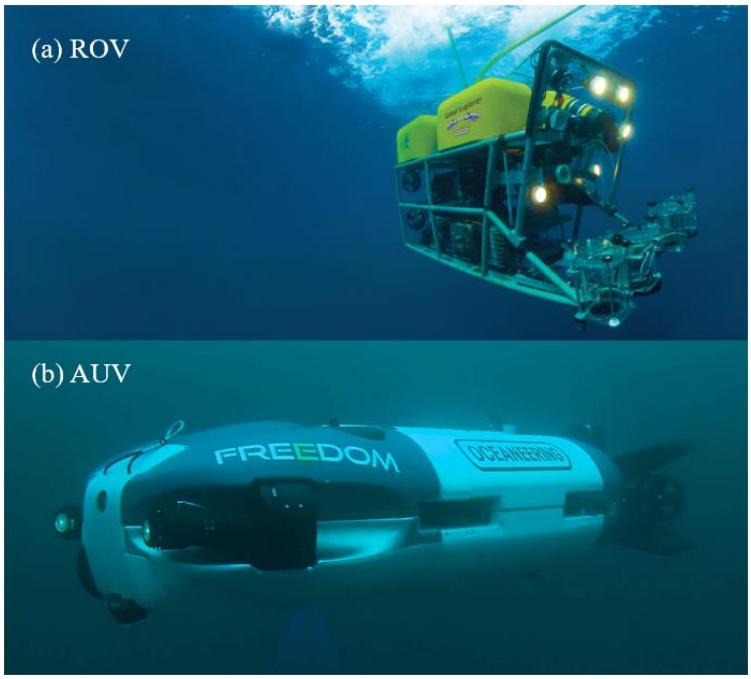

Figure 1-1 ROV (up) and AUV (down) in the water (Oceaneering 2021)

A brief comparison of the important features in ROV and AUV is presented in Table *1-1* Comparison between ROV and AUV to

Table 1-1 Comparison between ROV and AUV

Feature	ROV	AUV
Controllability	More controllable; controlled remotely by operators	Without any manual intervention; controlled by a pre-set program
Working range	Limited due to tether length	No limitation
Ability	Multifunctional with different tools	Commonly with single function
Dynamics	Generally fully-actuated	Generally underactuated

Accurate, optimal and robust navigation is crucial for these vehicles to operate effectively underwater. During some operations, such as dynamic positioning, path tracking or target following, the ROV would also work like an AUV controlled by a pre-set program. Given above, making a ROV have functions from both ROVs and

AUVs can be a feasible solution for most of the underwater unmanned missions, this is the motivation of this thesis work. As the objective of this work has been determined to be modifying a ROV into an autonomous vehicle in 1.3 below, the concept introduction of UUVs will then focus on the of ROVs.

Based on the purpose of use and functions, ROVs can be generally categorized into two classes: inspection-class (observation-class) ROVs and intervention-class (work-class) ROVs. Regarding to the size and weight, inspection-class ROVs can be further subdivided into micro ROVs and medium sized ROVs; intervention-class ROVs can be subdivided into light work-class ROVs and heavy work-class ROVs.

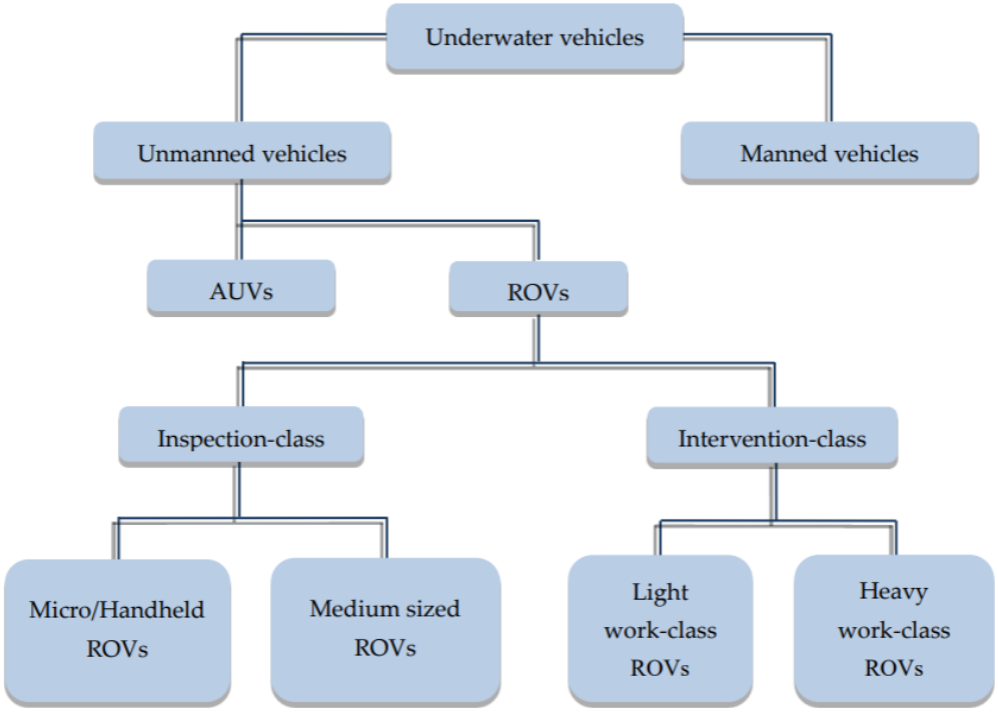

Figure 1-2 Outline of underwater vehicles (Capocci 2017)

Inspection-class ROVs are generally small and light, so that they can often be deployed and recovered by manpower. Limited to the size and weight, their maximum diving depth is commonly less than a few hundred meters and maximum propulsion power is usually at the kilowatt scale. Micro ROVs typically weigh between 3 kg and 20kg, and medium sized ROVs weigh from 30 kg to 120 kg. Intervention-class ROVs are relatively large and heavy, they generally weigh from hundred kilograms to thousands

of kilograms. Among them, the heavy work-class ROVs can weigh up to 5000 kg. A Launch and Recovery System (LARS), along with a Tether Management System (TMS), is equipped to deploy and recover the intervention-class ROV, because it is impossible to do this with manpower. Intervention-class ROV can generally operate as deeply as 3000 meters, for some heavy work-class ROVs, they can even dive to a maximum depth of 5000 meters.

According to the category in Figure *1-2* above, the prototype vehicle BlueROV2 which has been selected as the experimental platform in this thesis is a kind of micro ROV. BlueROV2 (base version) as shown in Figure *1-3* is produced by Blue Robotics and it is popular in scientific research as it is affordable and high-performance. For example, BlueROV2 has been used as an imaging tool for the exploration of coral bleaching by Taegue. Although BlueROV2 is a tethered underwater vehicle, it still has the possibility to be easily modified into an autonomous vehicle due to its utilisation of open-source software. This provides a fully-featured open-source solution for ROVs and AUVs allowing the BlueROV2 to work with a wide variety of hardware such as sonar sensors, cameras and inertial navigation system. Autonomous capabilities can be implemented on the BlueROV2 with custom-written code utilising these hardware. For example, Ludvigsen et al. discussed the implemention of computer vision assisted naviation in BlueROV2. More details of BlueROV2 are presented in Chapter 2.

Figure 1-3 BlueROV2 base version (BlueRobotics 2021)

1.2. Dynamic Positioning

Dynamic Positioning (DP) is an automatic system to achieve station keeping for surface and underwater vehicles or structures. For marine structures or large vessels, DP is generally a complementary to the mooring system. But for the BlueROV2 used in this thesis, DP is the only way to make it keep at desired location and heading. DP is accomplished by controlling propellers and thrusters to drive the vehicle against environmental loads like winds, waves, currents. The DP problem which is going to be studied in this thesis report is illustrated in Figure where the BlueROV2 is subjected to a gaussian current coming in at an aribitary gaussian heading.

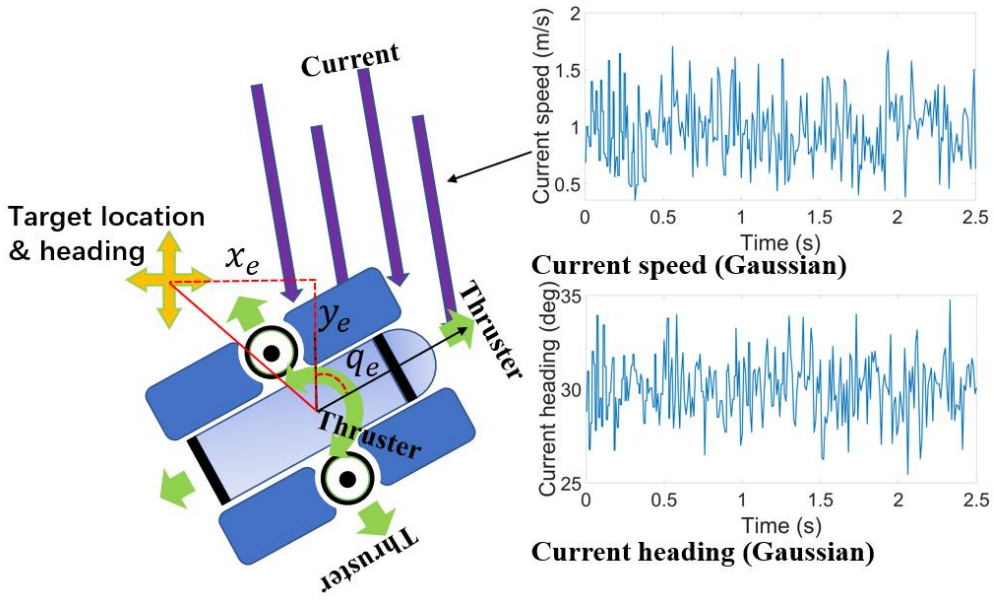

Figure 1-4 Dynamic positioning of BlueROV2 subjected to a current coming at an arbitrary heading

In general, the DP system is totally conducted by computer programs without any manual intervention. So, the system must be designed accurate, optimal and robust. The most two important issues in DP system design are state observation and control design. The realization of state observation/estimation firstly requires collecting information from wind sensors, geomagnetic sensors, sensors in inertial navigation system (INS) like acceleration sensors and gyrocompass, and global position system (GPS) etc. Then, an estimate algorithm will process the signals form various sensors and pass the position

and heading information as a result to the DP system. So the accuracy of sensors and optimality of estimate algorithm are the keys of state observation/estimation. However, this is not the emphis in this thesis work, so the noise and error of state observation are just supposed values in a reasonable range in 5.4. The central challenge in control design of DP system is the tuning of controller and that is the main content in this thesis work. How to carry out the tuning and how to qualify its optimality and robustness are both specified in the following section.

1.3. Objective and Approach

1.3.1. Objective of the thesis

According to the background above, the objectives of this thesis work are set in two steps as:

- Building up a proper 2D planar dynamic model of BlueROV2 based on the data and description in Chapter 2. This mathematic model should be able to accurately reflect the dynamic state on a horizontal x-y plane of BlueROV2.
- Creating a closed-loop DP control system based on the open-loop plant model of BlueROV2 mentioned in last step. Tuning the controller to make this DP control system robust and optimal.

1.3.2. Approach

Given the objectives above, the implementation of modeling and tuning have been selected to be carried out in software Matlab and the accompanying block diagram environment Simulink which is extensively use in model-based design work.

The simulation of DP control for BlueROV2 should be based on the fundamental principle proposed by Fossen and Johansen in 2006. As illustrated in Figure *1-5*, the control forces are generated by controller based on the feedback of ROV's state, and then the control allocation item will distribute these forces to actuators on ROV.

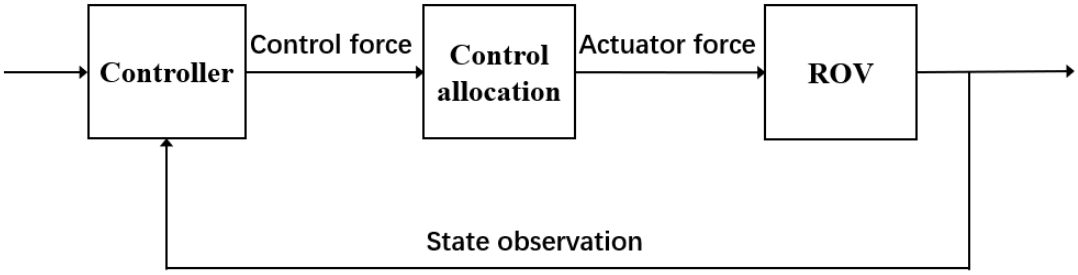

Figure 1-5 Diagram of ROV feedback control (Fossen 2006)

To simplify the work, the control allocation has not been set as the same as actual configuration of propellers in BlueROV2's DP control design. The block diagram of DP control for BlueROV2 in this thesis is shown as Figure *3-4* From open-loop control sysem to closed-loop control system with PID controller in Chapter 3 below. The commonly-used feedback control algorithms or controller in ROV's automatic control are proportional integral derivative (PID) control, linear quadratic regulator (LQR) and sliding mode control (SMC) etc. Considering the mathematical complexity of the model, and computing power requirement and complexity of tuning of each controller, a PID controller has been finally adopted in this thesis, and more details can be found in 3.3.

Classical tuning methods for PID controller are trial and error tuning method, Ziegler-Nichols tuning method, Cohen-Coon tuning method etc. As the tuning is carried out in Matlab Simulink, a powerful tool, Matlab PID tuner application can be utilized. The graphical user interface (GUI) of that is shown in Figure *1-6*. With Matlab PID tuner, the system performance of the controller with a step response can be easily observed. So, the approach of PID tuning in this thesis is changing the PID parameters (gains) depends on the system performance. It can be considered as a kind of trial and error tuning method, and more details is discussed in Chapter 4.

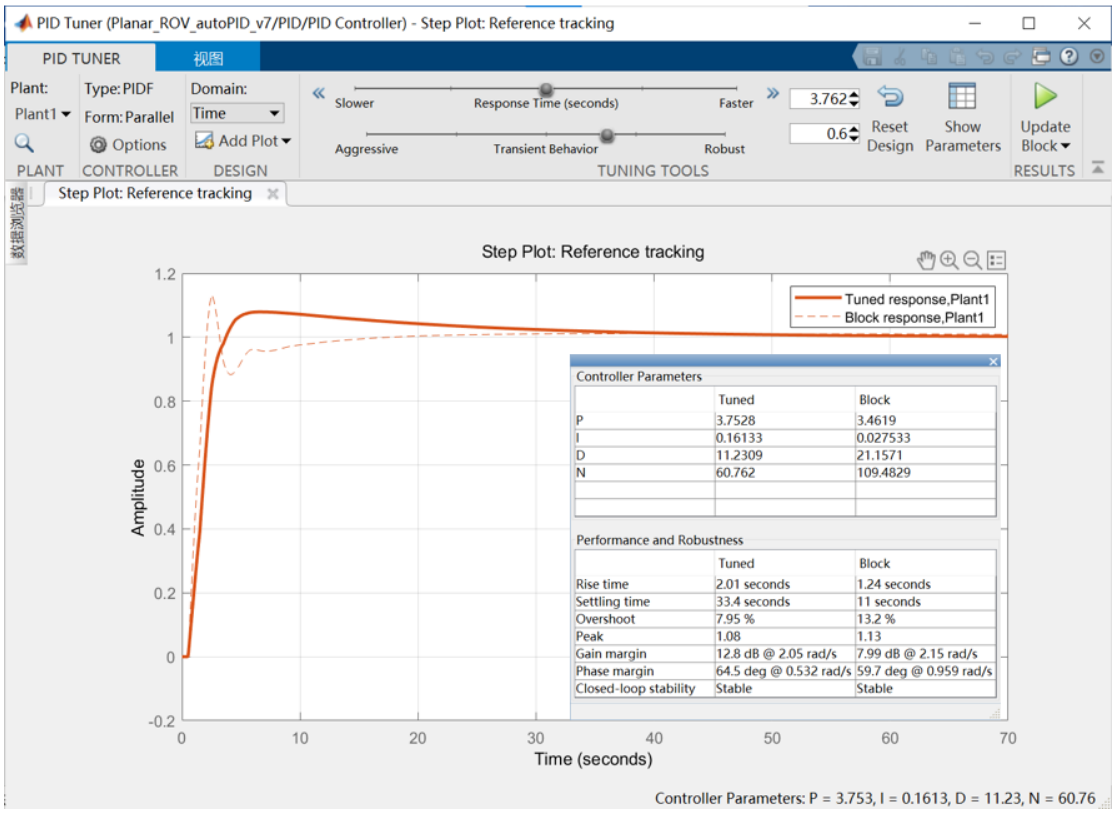

Figure 1-6 GUI of Matlab PID tuner

The robustness of the DP control is examined by comparing the simulation results from a set of representative cases with various scenarios.

1.4. Outline of Thesis

Chapter 2 presents the detailed information of BlueROV2 which is the experimental platform of the thesis. Some assumptions of BlueROV2 have been made to simplify the mathematic and system design, for example, the added mass inertia and damping coefficient are ‘guess’ values. A table containing the parameters which have been used in the modelling is also given in this chapter.

Chapter 3 introduces all the theories applied in the following modelling and tuning works. This contains the reference frames which have been used to present the location and heading of BlueROV2, equations of motion as the mathematic foundation of dynamic model construction, concepts of PID control as the foundation of DP control system design and controller tuning.

Chapter 4 presents the PID control tuning method which is applied in this thesis and the tool used to implement the tuning. The desired result of tuning is also contained in this chapter.

Chapter 5 shows the simulation model in Simulink. The content includes an overview of the whole DP control system for BlueROV2 and the internal structure of sub-systems that have details to get aware of.

Chapter 6 lists out the cases setting of various scenarios for simulation.

Chapter 7 concludes the overall results and the discussions on the results from various aspects.

Chapter 8 summarizes a conclusion for the whole thesis work and presents suggestions for further work.

In the end, a draft of COTech conference paper based on the same work has been attached in Appendix.

Chapter 2 Description of BlueROV2

The BlueROV2 used in this paper and previously presented in Figure *1-3* is the base version offered by Blue Robotics. It is a micro observation class ROV that can operate up to 100 m. It is equipped with four horizontal and two vertical T200 thrusters which allows propulsion in 6 independent DOFs. The thrustor configuration is presented in Figure *2-1*. These thrusters can provide a maximum of propulsion of 88.3 N, 88.3 N, 68.7 N in surge, sway and heave motion respectively.

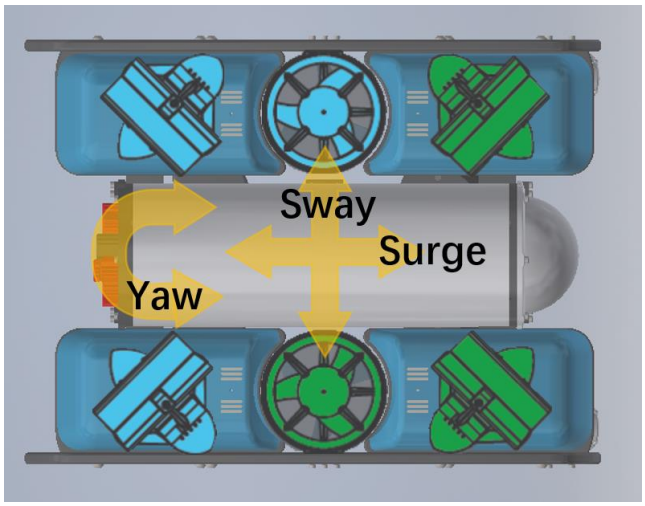

Figure 2-1 Thruster configuration of BlueROV2 from top view. Green and blue represent counter-clockwise and clockwise propellers, respectively

The main BlueROV2 parameters are presented in Table *2-1*.

Table 2-1 Main BlueROV2 parameters

Parameters	**Symbol**	**Value**	**Unit**
Length	L	0.457	m
Width	W	0.338	m
Height	H	0.254	m
Mass	m	10.565	kg

Yaw moment	I_{zz}	0.201	kg · m
Surge added mass	I_{Ax}	10.565 approx.	kg
Sway added mass	I_{Ay}	10.565 approx.	kg
Yaw added mass	I_{An}	0.201 approx.	kg · m
Quadratic damping coefficient	C_D	0.5 approx.	-
Surge cross section area	A_x	0.048 approx.	m^2
Sway cross section area	A_y	0.10 approx.	m^2
Yaw cross section area	A_n	0.07 approx.	m^5
Surge thrust maximum	F_{x_max}	88.3	N
Sway thrust maximum	F_{y_max}	88.3	N
Yaw thrust maximum	T_{q_max}	17.5 approx.	N·m

BlueROV2 is driven by the open-source Ardusub software running on an open-source Pixhawk autopilot system. The PixHawk autopilot is a powerful open-source hardware platform that has an on-board inertia measurement unit (IMU) and multiple I/O ports and has been adapted for use in a wide variety of drones (air/land/sea). The IMU includes accelerometers, gyroscopes and compass which support the state observation of BlueROV2. Moreover, multiple external sensors can be connected to the PixHawk autopilot via I/O ports. A Raspberry Pi 3 is used as a companion computer to provide HD video streaming to the surface workstation via the tether and Fathom X interface. The wiring diagram of BlueROV2 has been given:

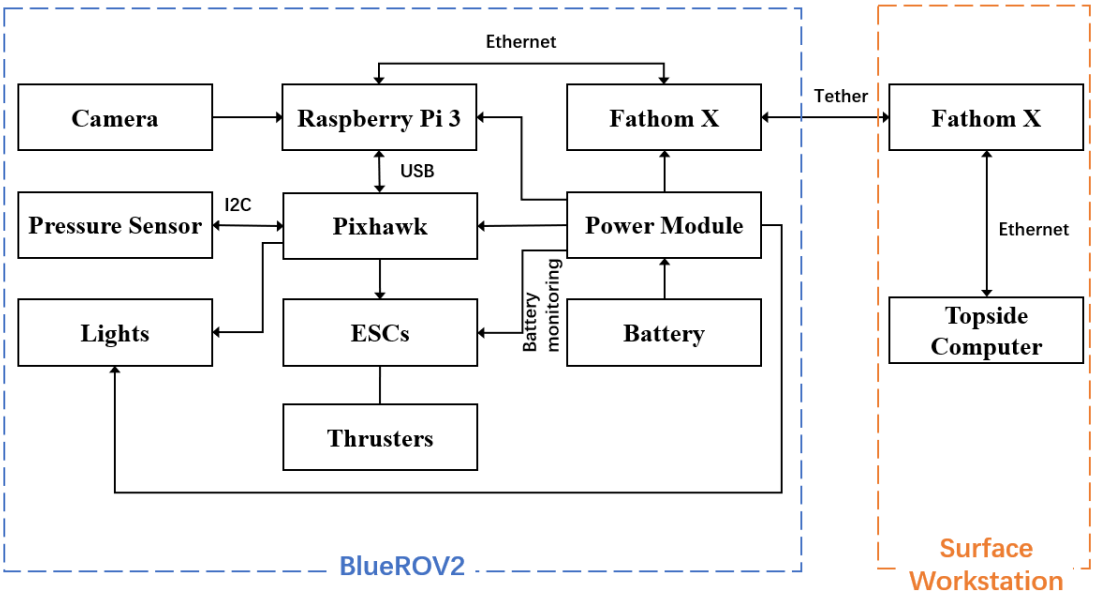

Figure 2-2 Wiring diagram of hardware on BlueROV2 and surface workstation

Chapter 3 Theory

As mentioned, this paper will focus on 2D planar dynamics, i.e., only x-y plane motions are considered and there is no heave, roll and pitch motions. In addition, the following assumptions are made:

- The BlueROV2 is assumed to be hydrodynamically symmetrical, i.e., there are no hydrodynamic coupling terms.
- The BlueROV2 is assumed to operate far away from the wave-affected zone, i.e., the load-effects of waves are negligible and only currents will be considered.

3.1. Reference Frames

3.1.1. Definitions

Since the work is going on with a 2D planar dynamic model, the real earth frames are not required. The following two frames have been introduced to present the location and heading attitude of ROV:

- North-East-Down frame (NED frame, n-frame): NED frame is the reference frame that people use to describe navigation information in their daily life, so it is also called navigation frame. The Origin O_n of n-frame is on the surface of earth. Axis X_n (N) points towards due north direction and Y_n (E) points towards due east direction. X_n-Y_n plane coincides with the tangent surface of earth spheroid at Origin O_n, following the right-hand rule, axis Z_n (D)points downwards perpendicularly.

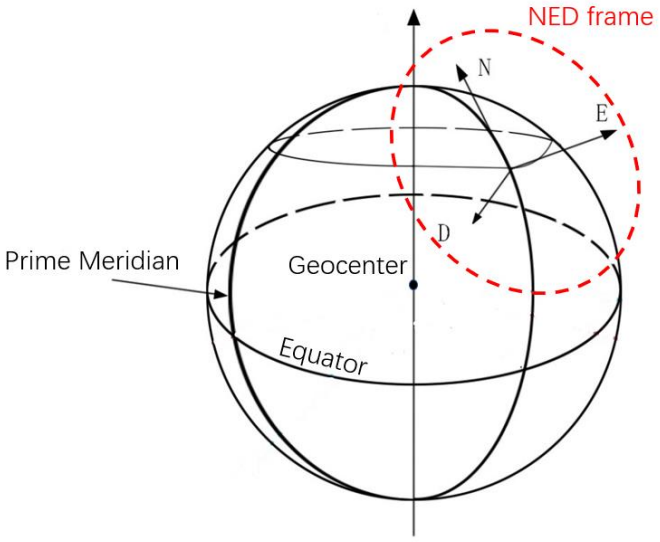

Figure 3-1 North-East-Down frame on the earth

- Body frame (b-frame): The b-frame is al frame fixed on BlueROV2. The origin O_b is defined at the geometric center of BlueROV2. Axis X_b points towards ROV's surge forward direction and axis Z_b represents the vertical downward direction from BlueROV2. Following the right-hand rule, axis Y_b points towards right side of the ROV.

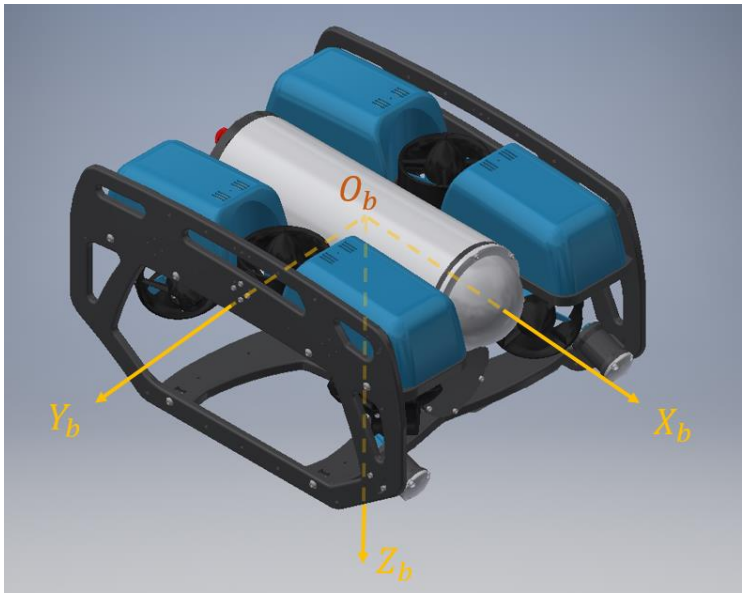

Figure 3-2 Body frame on BlueROV2

3.1.2. Expression of location and heading

As only x-y plane motions are considered in this thesis report, both n-frame and b-frame can be simplified into 2D frames on one plane. The transformation from a 2D frame to another 2D frame on the plane is very simple which only needs two displacements and one rotation. To present the location and heading of planar BlueROV2 model, n-frame

is supposed to be fixed. The displacements and rotation angle which has been taken place during the transformation from n-frame to b-frame are right the location and heading of BlueROV2 as shown in Figure *3-3* below.

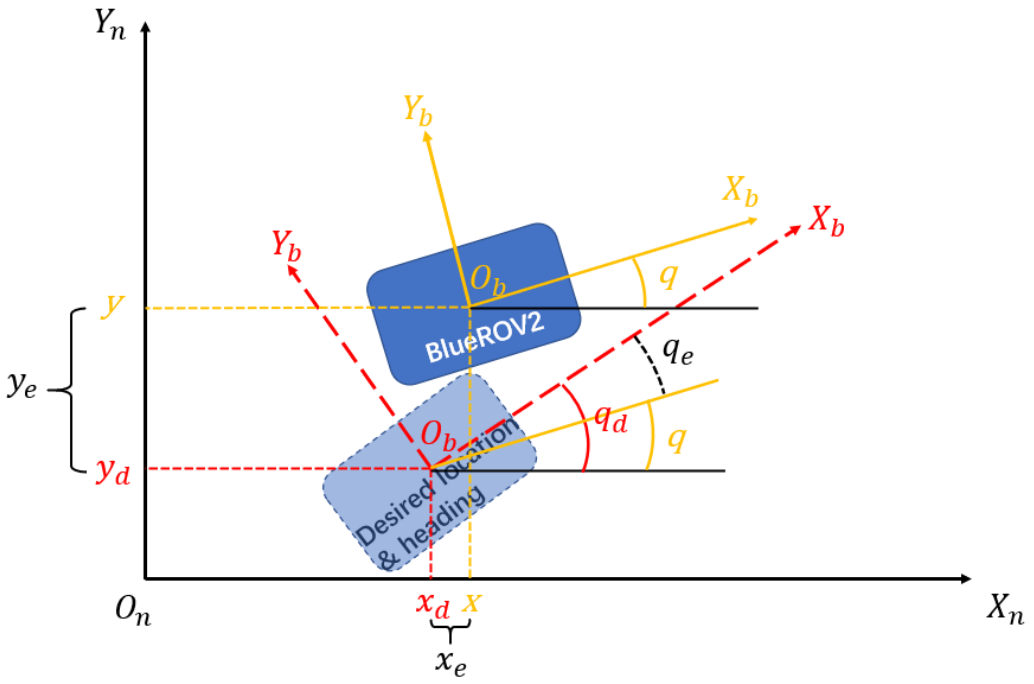

Figure 3-3 Interpretation of how location and heading of BlueROV2 and dynamic positioning error are expressed in n-frame.

Expressed in n-frame, *x* and *y* present the location of BlueROV2 and *q* presents the heading angle. Combing with the DP problem, $\boldsymbol{p} = [x \quad y \quad q]$ in yellow is the real time location state, and $\boldsymbol{p_d} = [x_d \quad y_d \quad q_d]$ in red is the desired location state. The bias between them which is defined as $\boldsymbol{p_e} = [x_e \quad y_e \quad q_e]$ is the input of the controller in 3.3 and Chapter 5.

3.2. Equations of motions

The equations of motions are the foundation to build up the mathematic dynamic model of BlueROV2. They describe the relationships among position $\boldsymbol{p}$, velocity $\boldsymbol{v}$, propulsions $\boldsymbol{\tau}$ and other external forces. The main equation of motions for a ROV can be expressed by the Newton-Euler equation as presented by Fossen:

$$\boldsymbol{M\dot{v} + C(v)v + D(v)v + g(\eta) = \tau} \qquad \text{Eq. (1)}$$

$$\boldsymbol{v} = \dot{\boldsymbol{p}} \qquad \text{Eq. (2)}$$

Where $\boldsymbol{M}$ is the mass matrix, $\boldsymbol{C(v)}$ is the Coriolis matrix, $\boldsymbol{D(v)}$ is the damping matrix, $\boldsymbol{g(\eta)}$ is the gravitational forces and moments, $\boldsymbol{v}$ is the velocity and $\boldsymbol{\tau}$ is the external driving forces. $\dot{\boldsymbol{v}}$ represents the acceleration and equals to the derivative of $\boldsymbol{v}$ with respect to time *t.*

For a 2D x-y planar dynamic problem without considering the transformation between real earth frame and navigation frame, $\boldsymbol{C(v)}$ and $\boldsymbol{g(\eta)}$ are zeros and Eq. (1) can be simplified and expanded to:

$$\begin{bmatrix} m + I_{Ax} & 0 & 0 \\ 0 & m + I_{Ay} & 0 \\ 0 & 0 & I_{zz} + I_{\mathrm{An}} \end{bmatrix} \begin{bmatrix} \dot{u} \\ \dot{v} \\ \dot{w} \end{bmatrix} + \frac{1}{2}\rho C_D \begin{bmatrix} A_x \\ A_y \\ A_n \end{bmatrix} \cdot \begin{bmatrix} |u| \\ |v| \\ |w| \end{bmatrix} \cdot \begin{bmatrix} u \\ v \\ w \end{bmatrix} = \begin{bmatrix} X \\ Y \\ T \end{bmatrix} \qquad \text{Eq. (3)}$$

Where $[u \quad v \quad w]^T$ are the velocities in surge, sway, yaw respectively, $[\dot{u} \quad \dot{v} \quad \dot{w}]^T$ are the accelerations in surge, sway, yaw respectively and $[X \quad Y \quad T]^T$ are forces and moment in surge, sway, yaw motion. $[I_{Ax} \quad I_{Ay} \quad I_{An}]$ are added mass components, ρ is the density of seawater, C_D is the drag coefficient and $[A_x \quad A_y \quad A_n]^T$ are the cross section areas for drag in three direction motions. Added mass on a rigid body is a virtual mass caused by the fluid around. In this study, added mass $[I_{Ax} \quad I_{Ay} \quad I_{An}]$ are assumed to be the same as the mass and inertia moment of BlueROV2 as listed in Table *2-1*.

Based on the assumption of hydrodynamic symmetry, the coupled terms have all not been considered. Correspondingly, the drag force can be regarded to be proportional to the square of the relative velocity between current and act in the opposite direction to the ROV's motion. Given the above, drag forces in surge, sway and yaw can be expressed respectively as:

$$X_D = -\frac{1}{2}\rho C_D A_x |u| u \qquad \text{Eq. (4)}$$

$$Y_D = -\frac{1}{2}\rho C_D A_y |v| v \qquad \text{Eq. (5)}$$

$$\psi_D = -\frac{1}{2}\rho C_D A_n |w| w \qquad \text{Eq. (6)}$$

The drag coefficients for three DOFs are all assumed to be 0.5 in this study. The cross section areas for each direction are listed in Table *2-1*.

3.3. Proportional-integral-derivative control

Proportional-integral-derivative (PID) control is commonly adopted in unmanned underwater vehicles and marine operation field. Two types of PID controllers are considered in this paper. One is a general PID controller that uses fixed controller gain values while the other one is a variable-gain (retuned) PID controller that will be retuned and adapt the new controller gains for different scenarios.

PID controller is a type of feedback controller that helps to reach a set point regardless of kinds of disturbances or variation in characteristics of the plant model. Using the PID controller, the open-loop BlueROV2 control system can transformed to a closed-loop control as shown in Figure 30. Based on the assumption of being hydrodynamically symmetrical, there are three uncoupled PID controllers used, one for each individual direction, i.e., surge, sway and yaw.

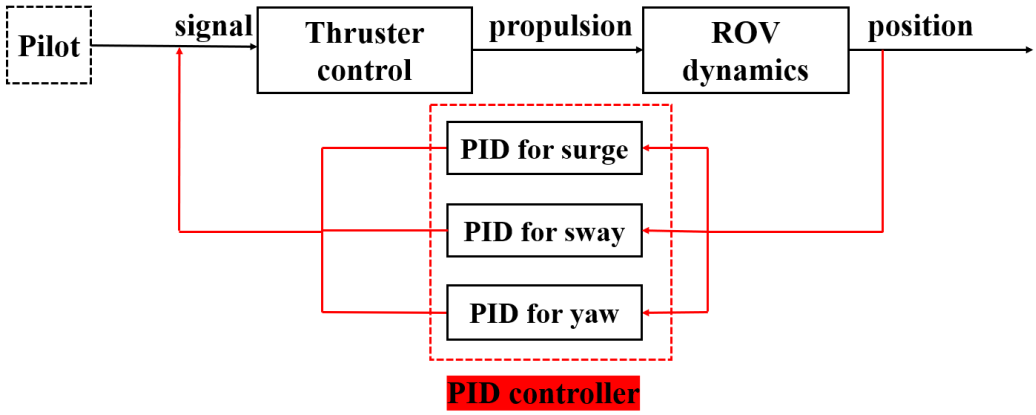

Figure 3-4 From open-loop control sysem to closed-loop control system with PID controller

The input for a PID controller is the error $e(t)$ between the measured process variable and the desired setpoint. The output $u(t)$ is produced with a correction

multiplied by a proportional gain (K_P), integral of the correction multiplied by an integral gain (K_I) and derivative of the correction multiplied by a derivative gain (K_D). The proportional gain (K_P) is simply used to multiply the input $e(t)$, the magnitude of K_P determined the general magnitude of the output. The integral gain (K_I) is used to multiply the accumulation of the recent errors over time which is in a form of integral. A proper K_I can help get rid of the steady state error, and help the system be able to reach some desired set point. The derivative gain (K_D) is used to multiply the derivative of error with respect to time. The derivative component contributes to the reaction to the rate of error changing, it makes the output match the desired value better. As described above, the overall function of PID controller is given below:

$$u(t) = K_p e(t) + K_i \int_0^t e(t)\,dt + K_d \frac{de(t)}{dt} \qquad \text{Eq. (7)}$$

In this study, $e(t)$ is the errors $[x_e \quad y_e \quad q_e]$ between the measured position of BlueROV2 $[x_m \quad y_m \quad q_m]$ and coordinate of the desired point $[x_t \quad y_t \quad q_t]$. The output is the thruster forces signal $[F_x' \quad F_y' \quad T_q']$ used to control the BlueROV2 to approach the target. Since the input and output in this control system are both 3-dimensional, and each two of three components are uncoupled. As mentioned above, the PID controller used in is decentralized into 3 sub-PID controller for x_e & F_x', y_e & F_y' and q_e & T_q', respectively. Tuning of this ROV motion control system involves the controller gains of individual PID controllers in surge, sway and yaw, i.e., their corresponding K_p, K_i and K_d values. As mentioned, two tuning methods are investigated in this paper. The first tuning method involves using a single set of K_p, K_i and K_d values for the whole system running process after proper tuning. The second tuning method uses K_p, K_i and K_d values that are retuned for each load case. In this way the control gains can be in theory adapted to different types of environmental loads and noise level.

Chapter 4 Tuning and desired system performance

The tuning tool used in this study is the Matlab PID tuner which works by principle summarized by Åström (2006). The PID tuner uses a system model linearized at an operating point for tuning. By changing the Bandwidth and Phase margin setting in frequency domain, the tuner will derive the corresponding controller gains automatically and also plot out the system impulse response. In this study, rise time (T_{rise}), setting time ($T_{setting}$), percentage overshoot (PO) and gain margin (γ) are used performance indicators. These are briefly discussed in the following and presented in Figure *4-1*.

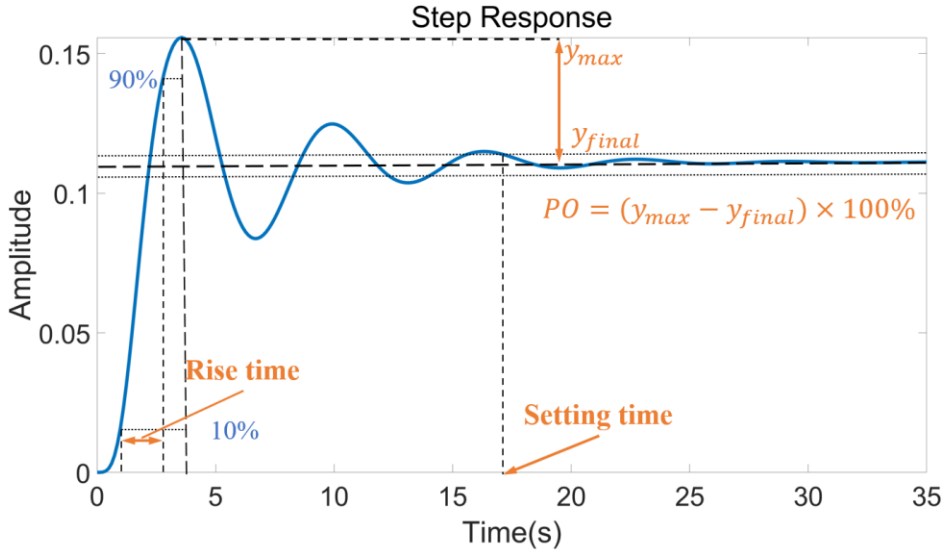

Figure 4-1 Rise time, setting time and overshoot in a step response

Rise time is defined as the time period for the system to rise from 10% to 90% of the steady state value. Rise time represents the respond speed of the system. It is desired to have a quick response, i.e., below 3 seconds for the BlueROV2. Setting time of a system is the time it takes for the error $e(t)$ to fall below 2% of the peak value of $e(t)$. A setting time reflects the ability of the system to stabilized. It is desired that the settling time of the BlueROV2 be less than 50 seconds. Percentage overshoot in a control system is the percentage of the maximum peak value of the response exceeding the final, steady-state value as expressed in Eq. (8). A larger overshoot represents more

potential oscillation or less stability. It is desired to have an overshoot below 50% in this study. The gain margin is the difference between 0 dB and the gain at the phase-cross-over frequency which is at the phase equals to -180 degree. A larger gain margin means a more stable system. When the gain margin becomes negative, the system is unstable. Gain margins in the interval of $[5, 30]$ dB is desired for the BlueROV2.

$$PO = (y_{max} - y_{final}) \times 100\% \qquad \text{Eq. (8)}$$

The base case in this paper has the following two sets of tuning objectives:

- Balanced - rise time < 1.5 s, setting time < 30 s, percentage overshoot < 30 % and gain margin > 5 dB.
- Rapid-response - rise time < 1 s, setting time < 10 s.

Chapter 5 Simulink Implementation

5.1. Overview

The Simulink implementation is illustrated in Figure 28.

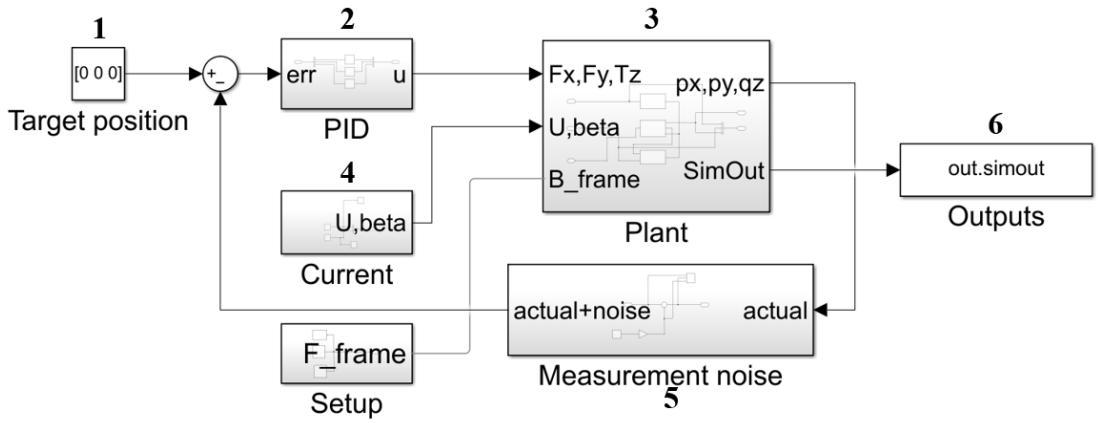

Figure 5-1 Simulink model diagram

The model consists of the following main blocks as labelled in Figure *5-1*:

- Block 1: Provides the coordinates of the set/desired location (x_d, y_d, z_d). In this thesis work, the desired location has been set as (0, 0, 0).
- Block 2: Contains the PID controllers. Each individual variable has an independent PID controller, i.e., a de-coupled PID control method is used.
- Block 3: Contains the plant model which considers the 2D planar dynamics of the BlueROV2.
- Block 4: Provides the gaussian current speeds and directions, and the global model set-up parameters.
- Block 5: Adds measurement noise into the ROV displacements measured from the plant model (Block 4).
- Block 6: Stores the simulation outputs.

Among these 6 blocks, some of them also has a complex subsystem, more details must be introduced to make the work proceed fluently and clearly.

5.2. Current

As shown in the Figure *5-2* below, the structure inside the current block is quite simple. It consists of two components: current speed and current heading, both are following a Gaussian waveform.

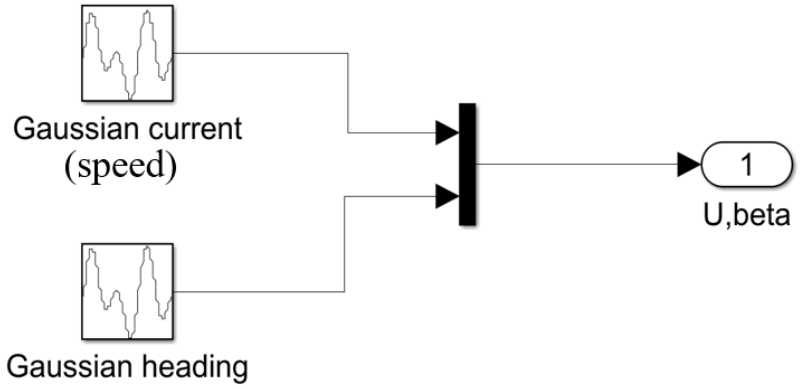

Figure 5-2 Internal structure of Simulink Current Block

The average values or expectations of Gaussian current speed and current heading is the variables in the cases study in Chapter 6. The standard deviations of Gaussian waves are expressed with coefficient of variation as shown:

$$\sigma = c_v \cdot \mu \qquad \text{Eq. (9)}$$

Where σ is the standard deviation of a Gaussian wave, μ is the average value of the same Gaussian wave, c_v is the coefficient of variation. Coefficient of variation is also a variable in the case study in Chapter 6.

The phases of Gaussian waves of current speed and heading are both set as 10.

5.3. Plant Model

5.3.1. Overview of plant model

The plant model (Block 3 in Figure 28) is presented in more details in this sub-section. A zoom view into the plant model is presented in Figure *5-3*.

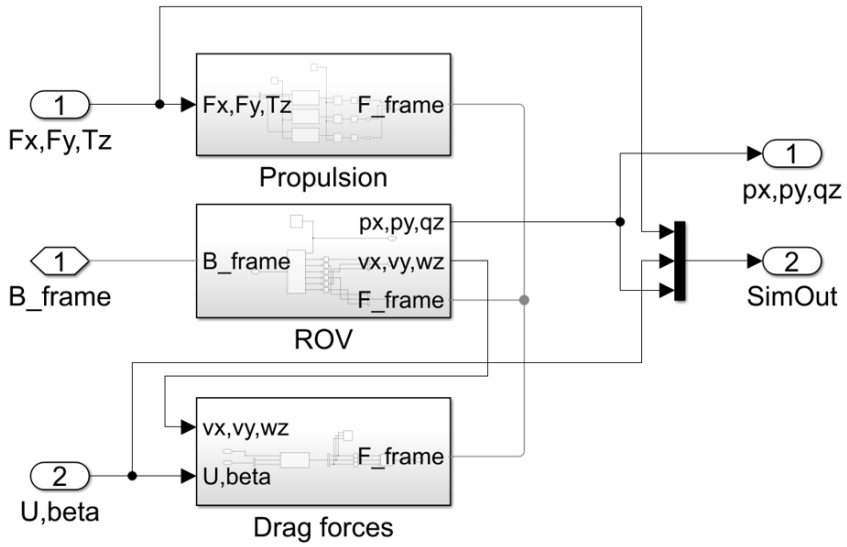

Figure 5-3 Plant model diagram

The plant model consists of three main blocks:

- Propulsion: This block models the propulsion forces. The block takes in the commanded forces and torque $[F_x' \quad F_y' \quad T_q']$ as inputs and applies them to the ROV block.
- ROV: This block contains a 2D planar rigid body with 3 degrees of freedom (x, y and n). Simulink will solve the equation of motion in accordance with Eq. (3) based on the forces and torque applied on the rigid body.
- Drag forces: This block calculates the drag forces and torque based on the current speed and ROV's velocities in accordance with Eq. (4), Eq. (5) and Eq. (6) and then applies them to the ROV block.

5.3.2. Propulsion

To simplify the work, the propulsion is not designed as the same as the configuration of thrusters on BlurROV2. Instead, only 3 items F_x', F_y' and T_q' which are commanded signals for thrust forces in surge, sway and torque in yaw come in from PID controller as input, and F_x, F_y and T_q which are real forces and torque generated by propellers in

surge, sway and yaw respectively have been passed to ROV block and applied on the BlueROV2 rigid body.

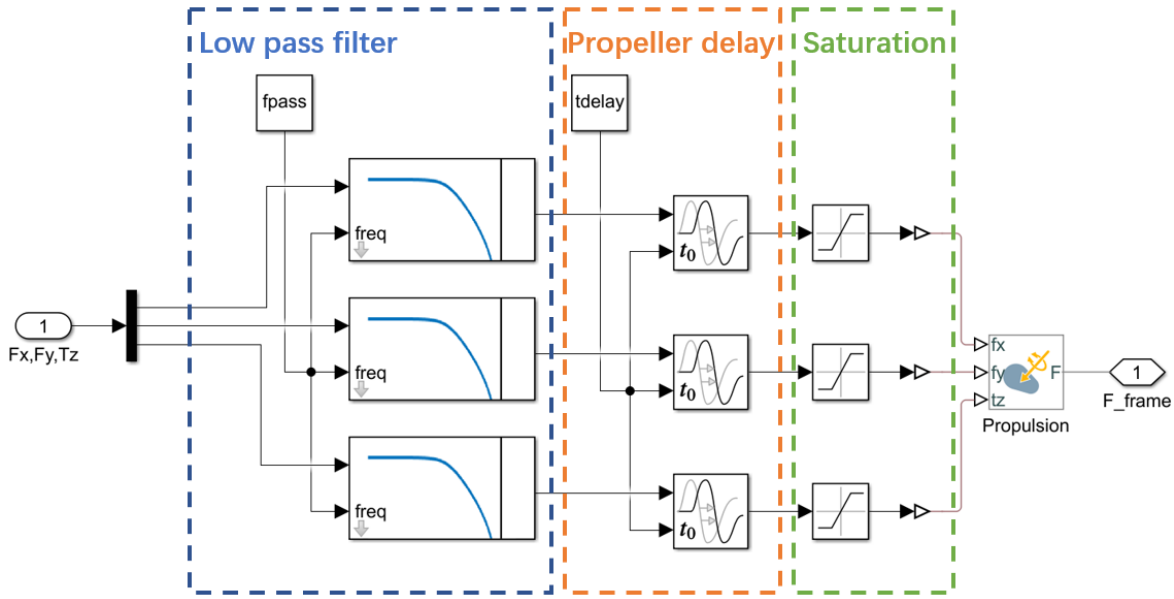

Figure 5-4 Internal structure of Simulink Propulsion Block

The Figure *5-4* above shows the internal structure of Propulsion block. As shown, three processes have been applied on the commanded signals to generate the final forces and torque acted on ROV.

Firstly to remove high frequency noise, a low pass filter with cut-off frequency of 1 Hz is applied on the commanded signals. This is to simulate the real digital signal passing to propellers, as the electrical machinery of propellers cannot process with the signals with too high frequency. Secondly, to simulate the physical delay of propellers, a variable time delay of 0.5 s is added to the commanded signals of thrust forces and torque. In the end, a saturation is set so that the forward and lateral thurst forces are saturated to [-88.3 ,88.3] N and the yaw moment is saturated to [-17.5 ,17.5] N·m in accordance with the physical limitations of the T200 thrusters.

5.4. Measurement Noise

Since there must be noise in the signal measured by sensors, a measurement noise block has been designed to add a noise on position information of BlueROV2 before it is passed to PID controller as input. The structure is as shown in the Figure *5-5* below:

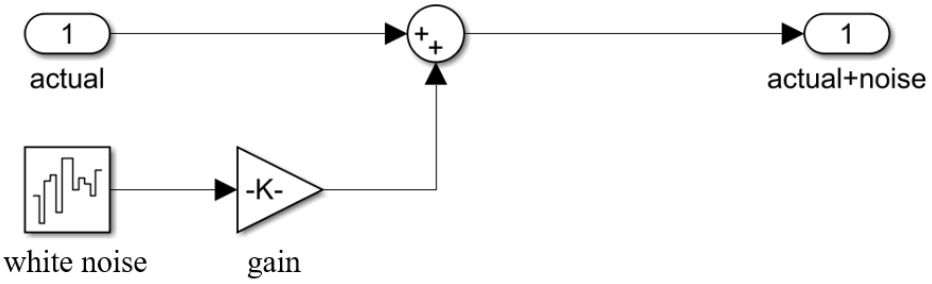

Figure 5-5 Internal structure of Measurement Noise Block

A white noise with power of 0.1 is added and a gain is set to control the noise level.

Chapter 6 Case Studies

To explore the effect of tuning, several cases with different current speed, heading, coefficient of variation (c_v) and measurement noise levels presented in *Table 6-1* are considered.

Table 6-1 Simulation cases

Case name	Current speed	Current heading	c_v	Control type	Noise
1-30-0.1-fx-lv1	1 m/s	30 deg	0.1	fixed	Level 1
1.5-30-0.1-fx-lv1	1.5 m/s	30 deg	0.1	fixed	Level 1
1-45-0.1-fx-lv1	1 m/s	45 deg	0.1	fixed	Level 1
1-30-0.15-fx-lv1	1 m/s	30 deg	0.15	fixed	Level 1
1-30-0.1-fx-lv2	1 m/s	30 deg	0.1	fixed	Level 2
1.5-30-0.1-tn-lv1	1.5 m/s	30 deg	0.1	tuned	Level 1
1-45-0.1-tn-lv1	1 m/s	45 deg	0.1	tuned	Level 1
1-30-0.15-tn-lv1	1 m/s	30 deg	0.15	tuned	Level 1
1-30-0.1-tn-lv2	1 m/s	30 deg	0.1	tuned	Level 2

The first case, i.e., 1-30-0.1-fx-lv1 is the base case. 'fixed' mean that the parameters K_p, K_i, K_d and filter coefficient *N* are fixed as the same as those tuned in the base case. 'tuned' means K_p, K_i, K_d and *N* are retuned to adapt to the current case. The objective in the retuning is to readjust the bandwidth and phase margin back to the same values as in the base case. Level 1 means that the gain for noise in surge direction = 0.001, gain for noise in sway direction = 0.001 and gain for noise in yaw motion = 0.00001. Level 2 means that the gain for noise in surge direction = 0.002, gain for noise in sway direction = 0.002 and gain for noise in yaw motion = 0.00002.

7.1. Base Case Gains

The controller gains for the Base Case (1-30-0.1-fx-lv1) are presented in *Table 6-2*and *Table 6-3* when balanced tuning and rapid-response tuning approaches are used, respectively. The tuning objectives were previously discussed in Chapter 4.

Table 6-2 PID gains for Base Case with balanced tuning

	K_p	K_i	K_d	N
Surge	3.4619	0.0275	21.157	109.48
Sway	10.901	0.7667	20.531	100.06
Yaw	0.0084	0.000043	0.3632	100.52

Table 6-3 PID gains for Base Case with rapid-response tuning

	K_p	K_i	K_d	N
Surge	14.936	0.1468	21.752	130.23
Sway	26.426	7.6454	22.681	118.54
Yaw	0.1260	0.00125	0.4818	135.08

A comparison of the time series of the x-position, y-position and heading angle when balanced and rapid-response tuning approaches are used is presented in *Figure 6-1*. As observed, the rapid-response approach leads to a faster system response; the orange line tends to lead the blue line in *Figure 6-1*. This effect is particularly pronounced in the heading angle response.

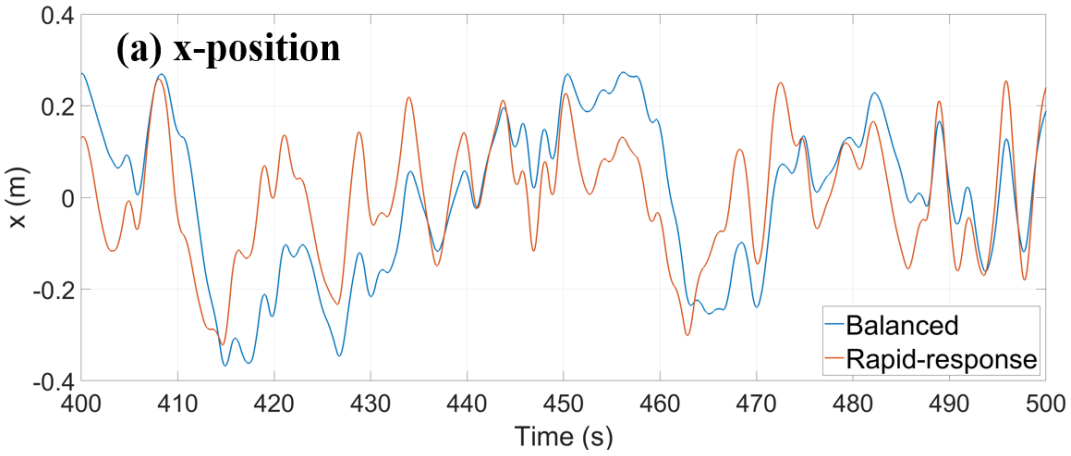

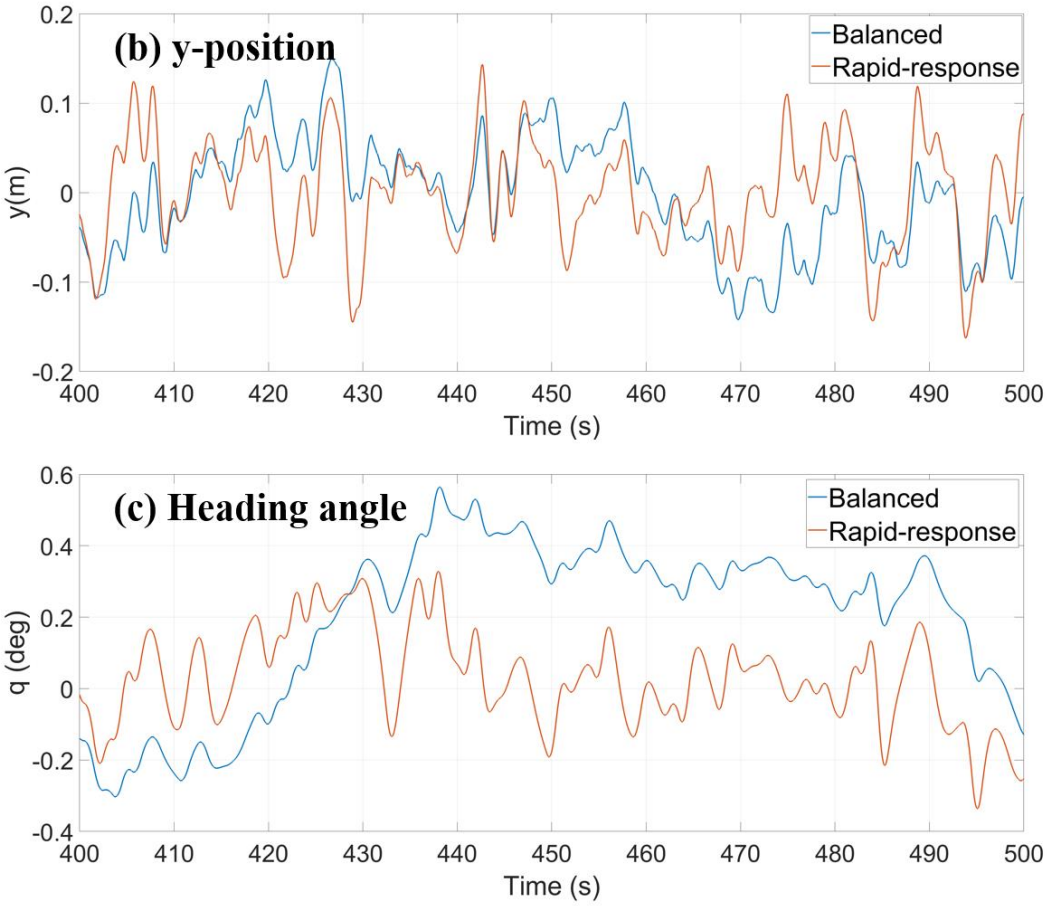

Figure 6-1 Times series of x-position, Base case, 1-30-0.1-fx-lv1, Balanced vs Rapid-response tuning approach.

7.2. Sensitivity study performed on Base Case

A sensitivity study is performed on the base case (1-30-0.1-fx-lv1) to explore the relationship between controller gains and performance in term of rise time, settling time, overshoot and gain margin. The study is performed on a model linearised at t = 450 s. The surge (x-dir) component is presented. The results are presented in *Figure 6-2*, *Figure 6-3*, *Figure 6-4* and *Figure 6-5*, for rise time, settling time, overshoot and gain margin, respectively.

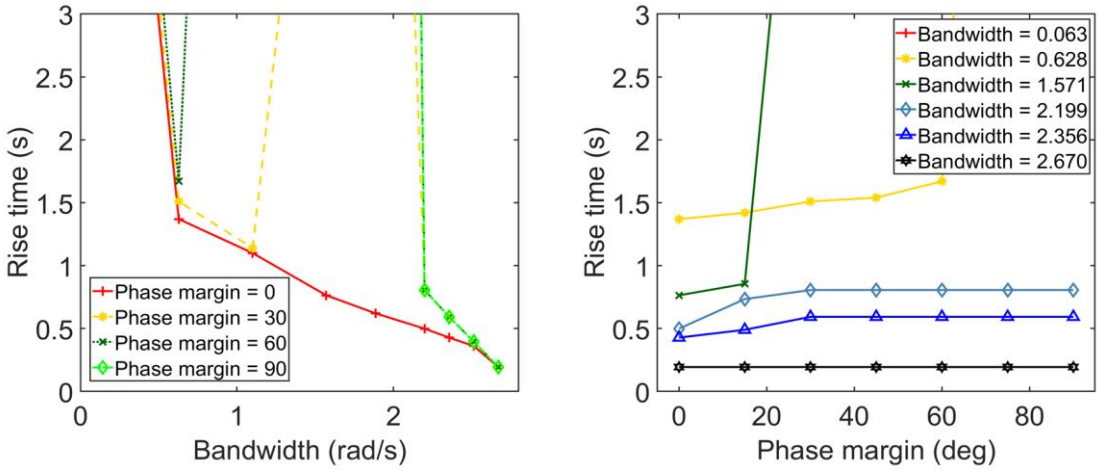

Figure 6-2 Base Case (1-30-0.1-fx-lv1), Surge (x-dir), Rise Time vs Bandwith and

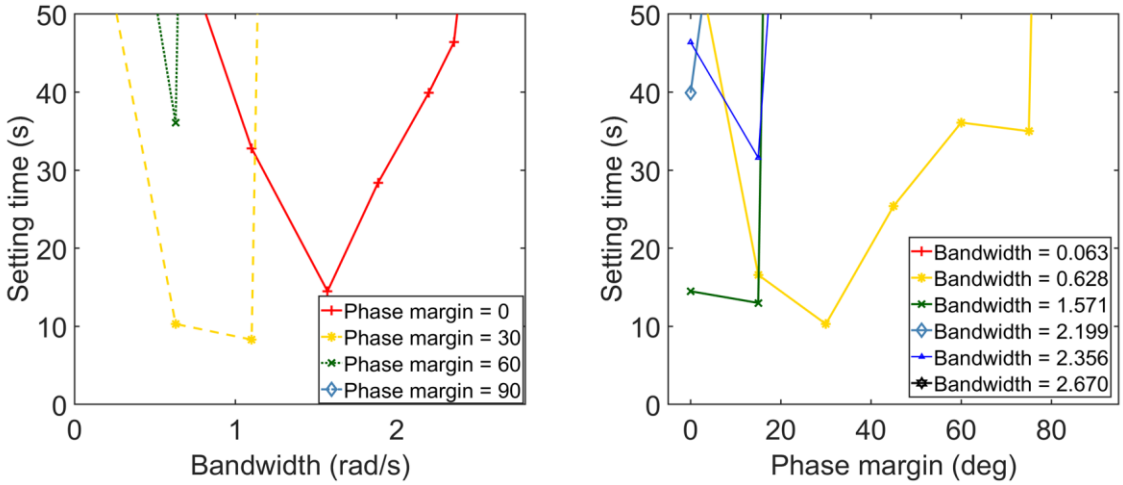

Figure 6-3 Base Case (1-30-0.1-fx-lv1), Surge (x-dir), Settling Time vs Bandwith and Phase Margin

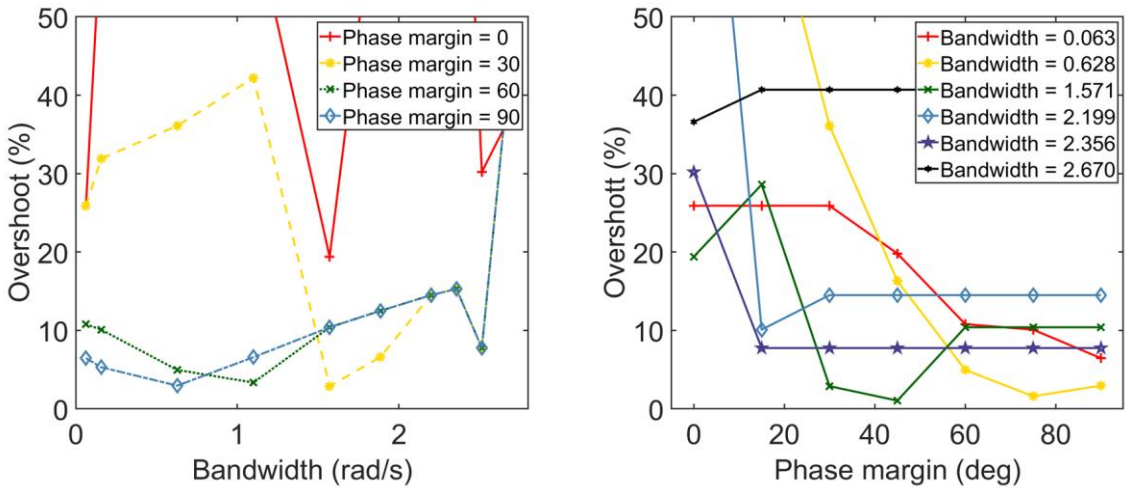

Figure 6-4 Base Case (1-30-0.1-fx-lv1), Surge (x-dir), Overshoot vs Bandwith and Phase Margin

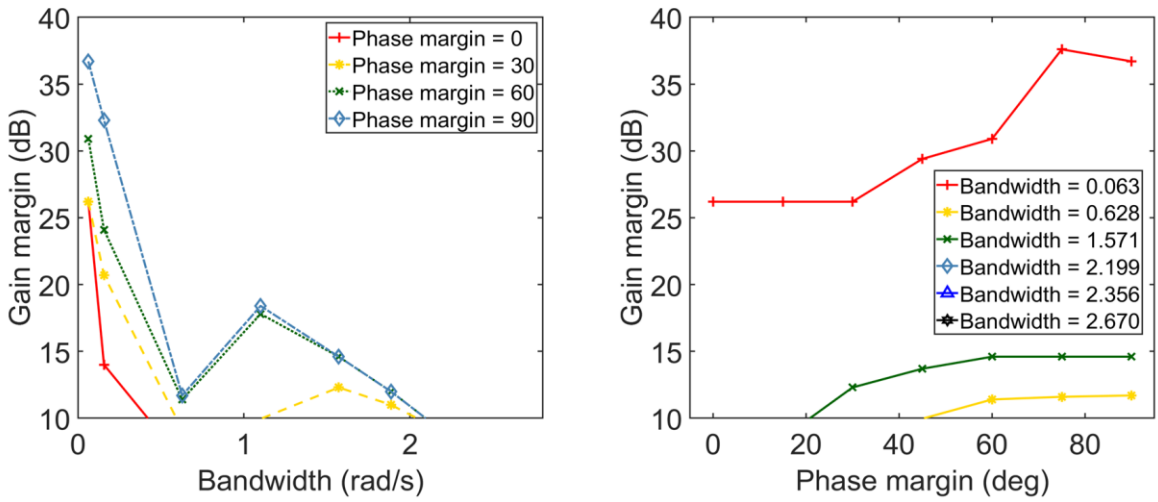

Figure 6-5 Base Case (1-30-0.1-fx-lv1), Surge (x-dir), Gain Margin vs Bandwith and Phase Margin

The following observations are made:

- Rise time decreases rapidly with increasing bandwidth, but is not affected by changes in phase margin.
- Settling time has a convave relationship (decreases then increases) with increasing bandwidth and phase margin.
- Overshoot is not affected by changes in bandwidth but decreases with increasing phase margin.
- Gain margin decreases with increasing values of bandwidth increasing but is not affected by changes in phase margin.

The above observations provide guidance for the subsequent controller tuning process that is performed in this thesis report.

7.3. Parametric correlation analysis

A parametric correlation analysis is performed to quantify the relationship between controller gains and performance variables. From the sensivitity study performed in Section 7.1, it is obvious that the relationships between these are nonlinear. Therefore, determination matrix which quantifies quadratic correlations is computed. The coefficient of determination, r^2 that relates variables x and y is expressed as:

$$r^2 = \frac{\sum(y_i - \bar{y})^2 - \frac{n-1}{n-2}(y_i - Y_i)^2}{\sum(y_i - \bar{y})^2} \qquad \textbf{Eq. (10)}$$

Where n is the total number of samples and $Y_i = ax_i^2 + bx_i + c$. The coefficient of determination has a value of 0 to 1. A value of 0 means no correlation, while a value of 1 means perfect correlation. The determination matrix is presented in Figure *6-6* Determination Matrix.

	Bandwidth	Phase margin	Rise time	Settling time	Overshoot	Gain margin	Kp	Ki	Kd
Bandwidth	1.00	0.00	0.22	0.01	0.01	0.66	0.16	0.10	0.16
Phase margin	0.00	1.00	0.22	0.20	0.48	0.10	0.47	0.42	0.00
Rise time	0.44	0.21	1.00	0.28	0.15	0.65	0.16	0.08	0.37
Settling time	0.05	0.34	0.35	1.00	0.27	0.07	0.24	0.27	0.13
Overshoot	0.00	0.40	0.17	0.27	1.00	0.14	0.23	0.23	0.03
Gain margin	0.64	0.10	0.34	0.08	0.19	1.00	0.21	0.16	0.53
Kp	0.14	0.39	0.14	0.07	0.22	0.28	1.00	0.63	0.57
Ki	0.03	0.33	0.07	0.08	0.25	0.13	0.71	1.00	0.00
Kd	0.97	0.01	0.17	0.01	0.04	0.51	0.10	0.04	1.00

Figure 6-6 Determination Matrix

The following observations are made:

- Rise time has an inverse quadratic coefficient of determination of 0.44 which means it has a somewhat quadratic relationship with bandwidth.
- The quadratic coefficients of determination between setting time and phase margin are 0.28 and 0.34 (inverse). This means a slight correlation.
- Percentage overshoot has quadratic coefficients of determination of 0.48 and 0.40 (inverse) with phase margin which means they are fairly correlated.
- The quadratic coefficients of determination between gain margin and bandwidth are 0.66 and 0.64 (inverse) which indicates a relatively strong correlaton.

The observations are summarized in Table 6-4. '+' indicates improved performance, '–' indicates impaired performance and '0' indicates no clear trend.

Table 6-4 Summary of observations from determination matrix

Performance variable	**Bandwidth**	**Phase margin**
T_{rise}	++	0
$T_{settling}$	+-	+-
PO	0	++
γ	-	0

7.4. Different simulation cases

The other different simulation cases presented in **Table 6-1** are studied in this sub-section using controller gains derived from both balanced and rapid-response approaches.

7.4.1. Step responses using Base Case gains

The system step responses when base case gains are used are presented in Figure 6-7and Figure 6-8 (next two pages) for the balanced and rapid-response tuning approaches, respectively.

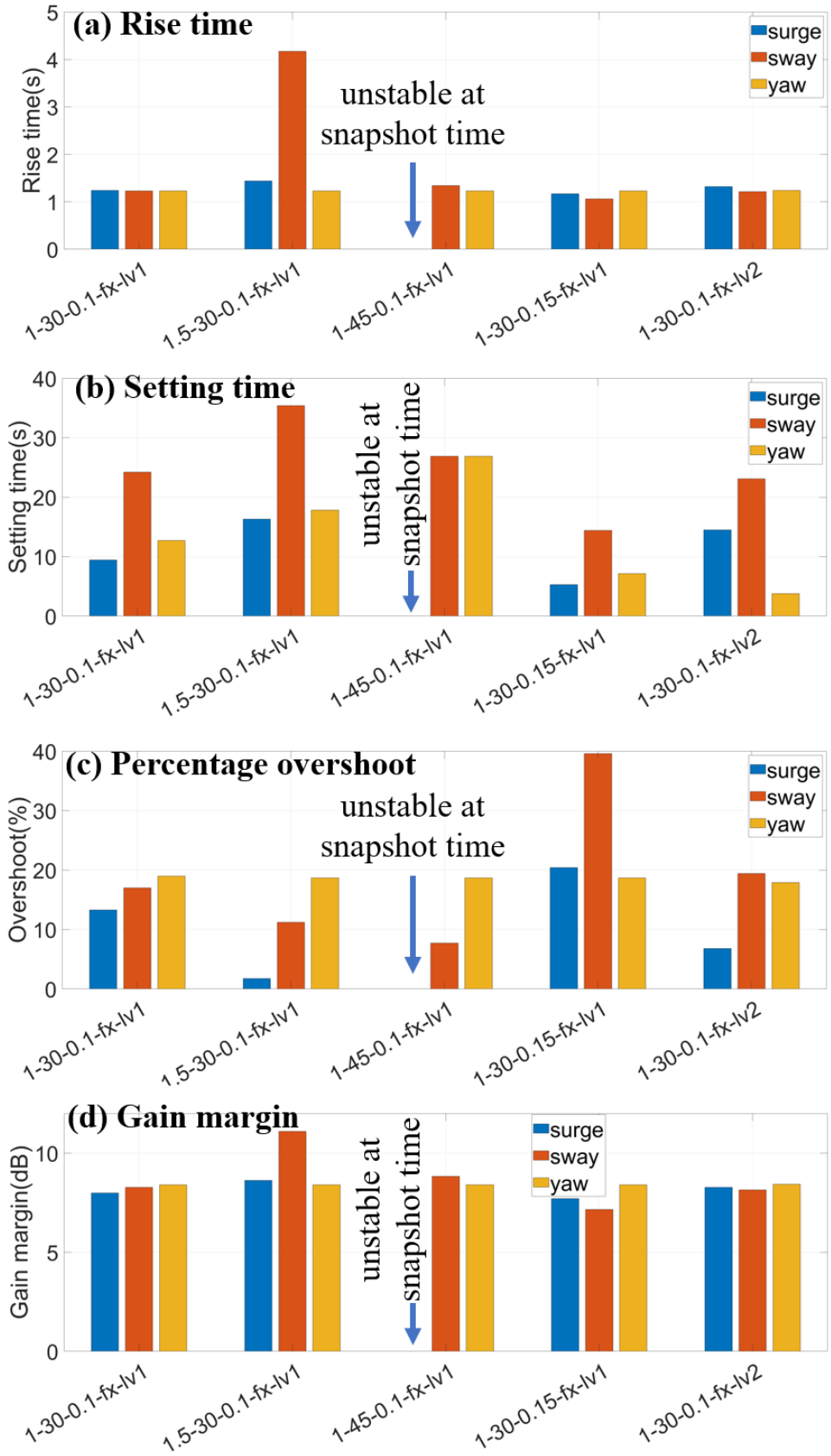

Figure 6-7 Balanced tuning approach, Step responses for different simulation cases, (a) Rise time, (b) Setting time, (c) Percentage overshoot and (d) Gain margin

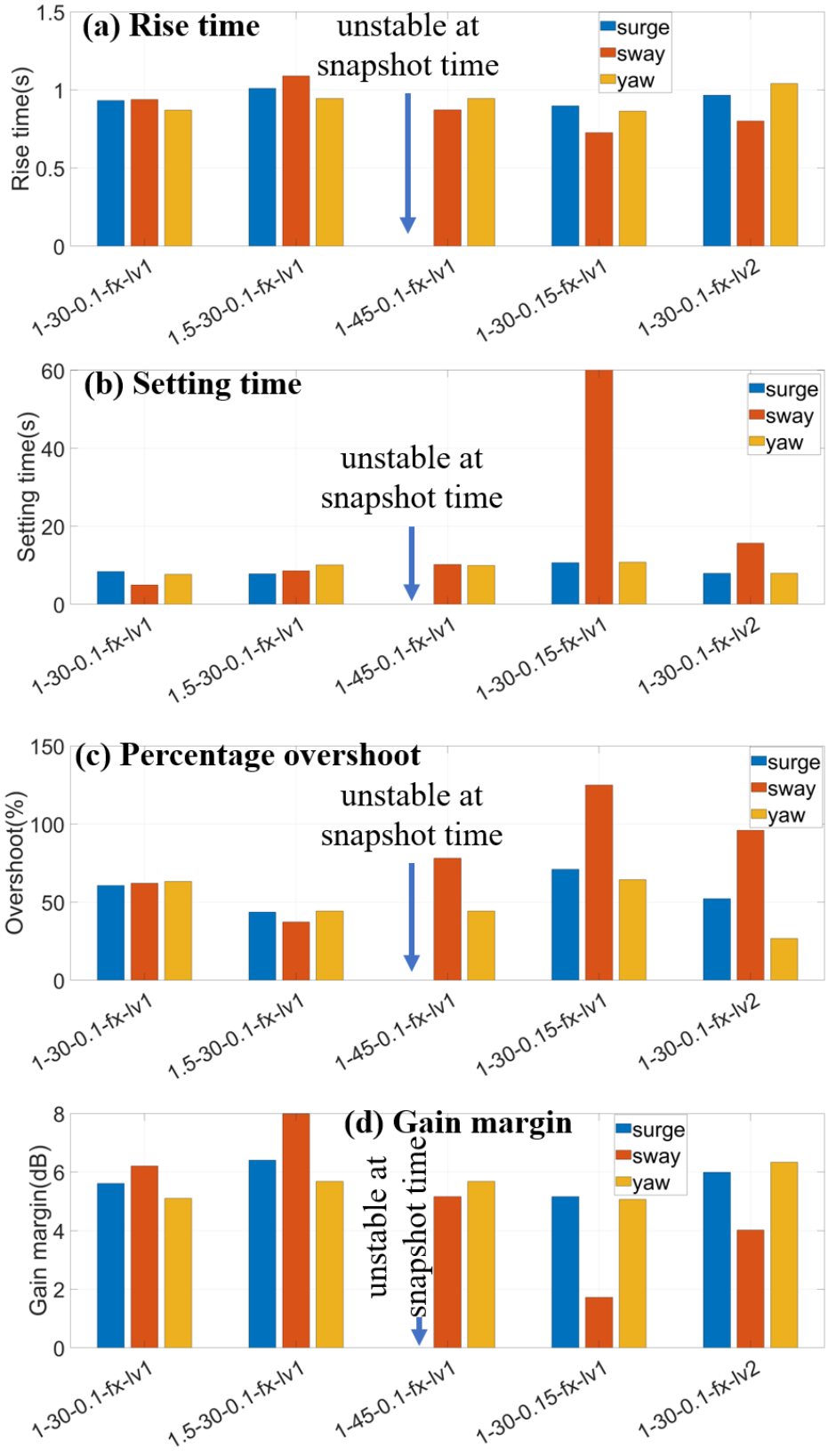

Figure 6-8 Rapid-response tuning approach, Step responses for different simulation cases, (a) Rise time, (b) Setting time, (c) Percentage overshoot and (d) Gain margin

In general, it is observed that the step responses are in general similar for the different cases except for the following cases:

- Surge component in 1-45-0.1-fx-lv1 and 1-45-0.1-tn-lv1: The system is unstable under a current heading of 45 degree.
- Sway component in 1.5-30-0.1-fx-lv1: The rise time increases when the balanced tuning approach is used.
- The settling time becomes are large as 60 seconds in 1-30-0.15-fx-lv1 when the rapid-response tuning approach is used.

To explore how these exceptions will affect the BlueROV2's performance, the time series of responses will be shown and discussed in the following sub-section.

7.4.2. Time series of responses

The time series of the corresponding responses of the cases presented in Figure 30 and Figure 31 are presented in *Figure 6-9*, *Figure 6-10* and *Figure 6-11* for the x-position, y-position and heading, respectively. In general, actual time domain responses show larger differences between the different simulation cases compared to that observed from the step responses presented in Section 7.4.1. This means that it is important not to purely and over rely on the step responses when tuning is performed. It is important to always test the system out in time domain and observe the actual time domain responses. It is also observed that the rapid-response tuning approach produces a somewhat poorer performance compared to the balanced tuning approach.

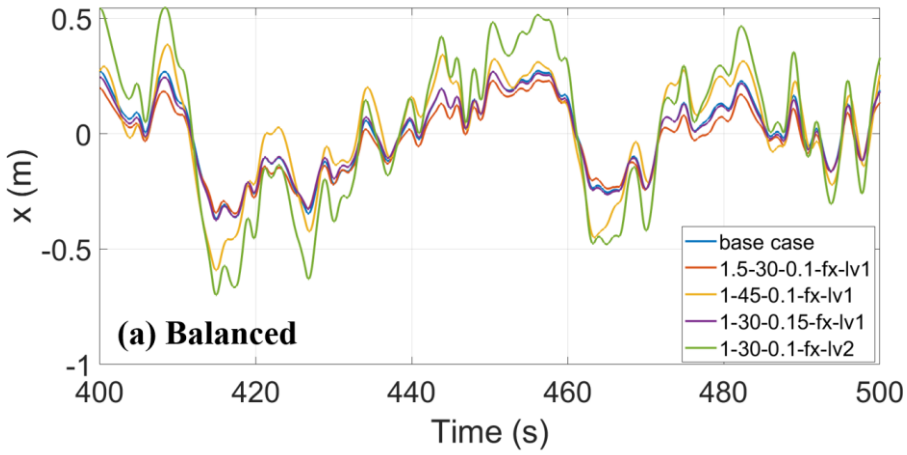

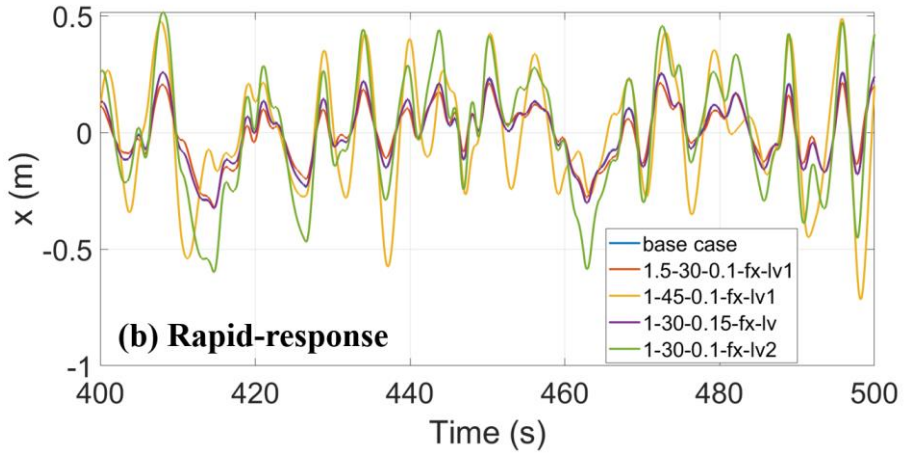

Figure 6-9 x-position for different simulation cases, (a) Balanced tuning (last page), (b) Rapid-response tuning

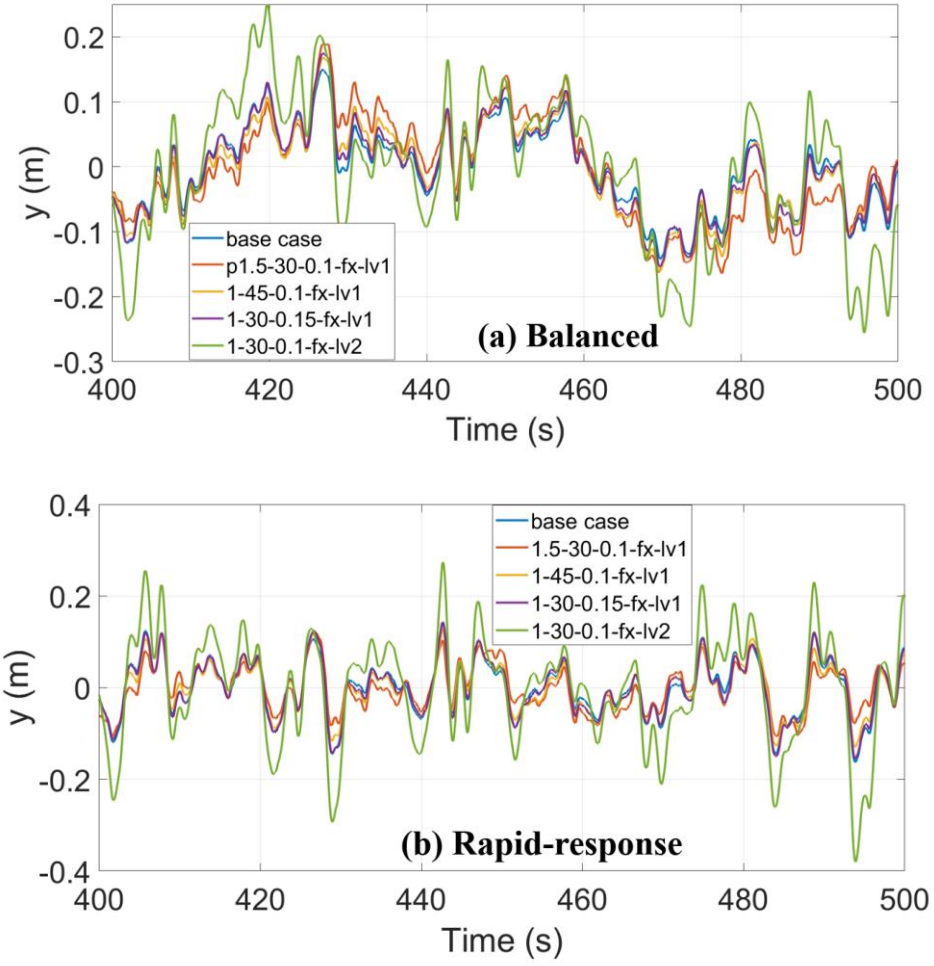

Figure 6-10 y-position for different simulation cases, (a) Balanced tuning, (b) Rapid-response tuning

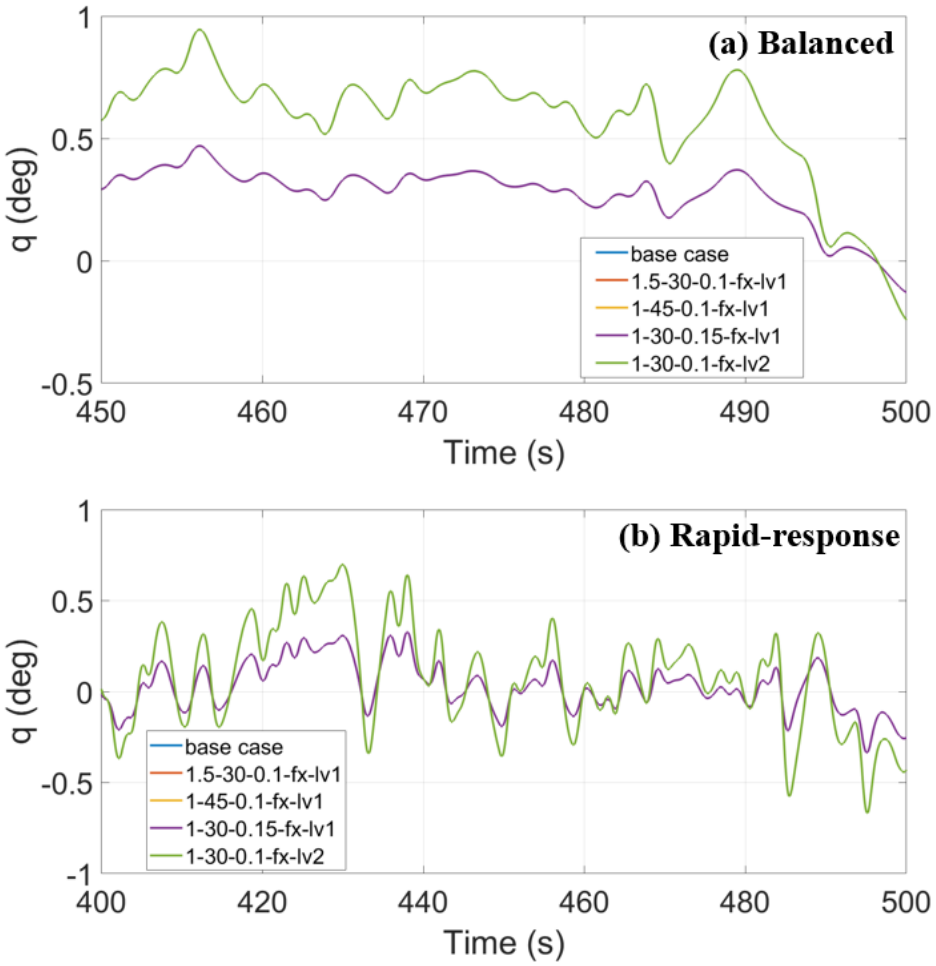

Figure 6-11 Heading for different simulation cases, (a) Balanced tuning, (b) Rapid-response tuning

7.4.3. Effect of re-tuning

In this section, improvements will be attempted on the time domain performances presented in 7.4.2 by performing re-turning for each simulation case. The system step responses when gains are retuned for each case are presented in Figure *6-12* and *Figure 6-13* for the balanced and rapid-response tuning approaches, respectively.

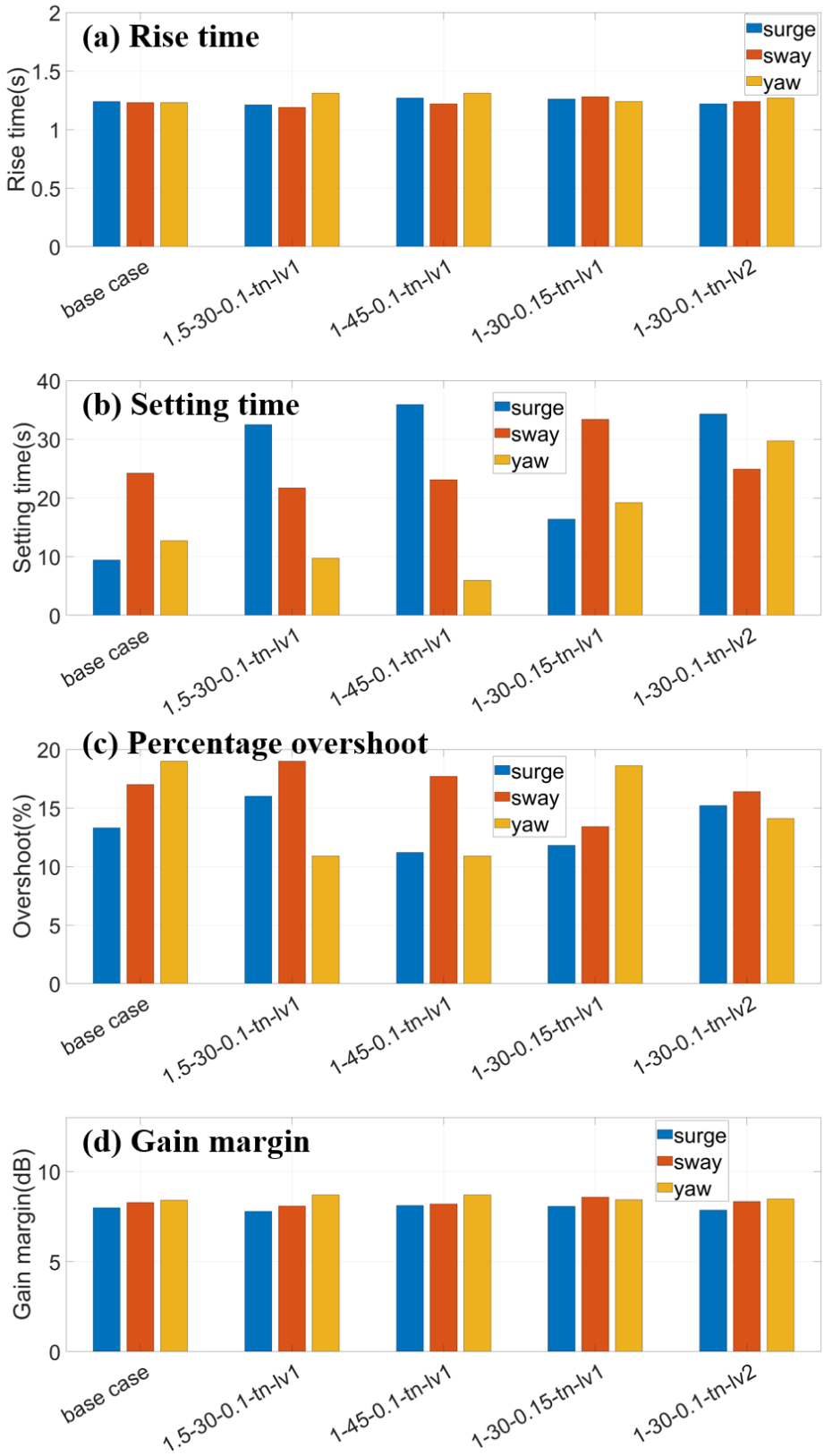

Figure 6-12 Balanced tuning approach, Step responses for different simulation cases, (a) Rise time, (b) Setting time, (c) Percentage overshoot and (d) Gain margin

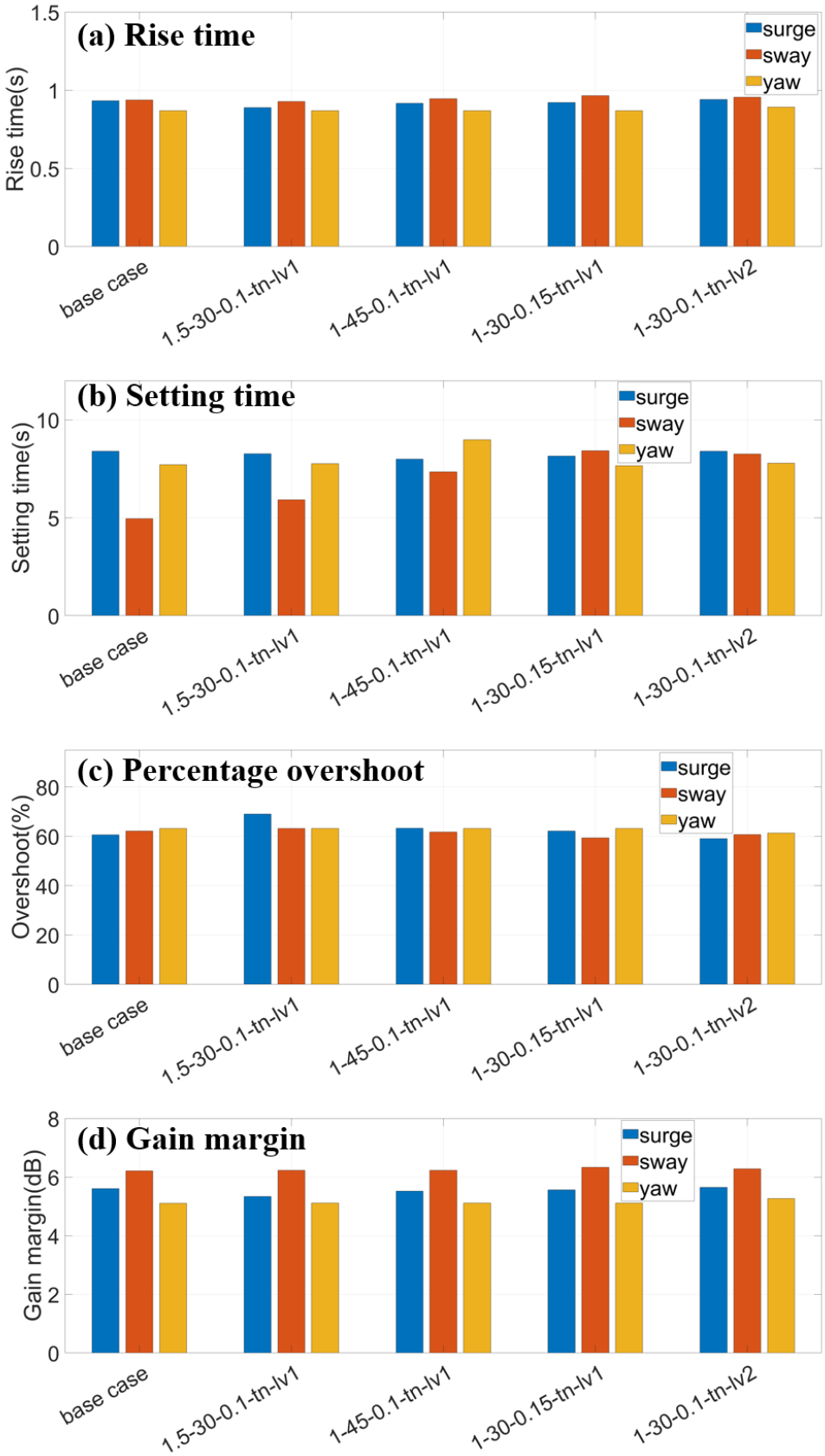

Figure 6-13 Rapid-response tuning approach, Step responses for different simulation cases, (a) Rise time, (b) Setting time, (c) Percentage overshoot and (d) Gain margin

It is obvious that the step responses with retuned PID controllers for the different cases vary less than that with fix-gain PID controllers.

The time domain responses are presented in Figure *6-14*, Figure *6-15* and Figure *6-16*, respectively for x-postion, y-position and heading. In general, it is observed that re-tuning the PID controllers leads to better performances.

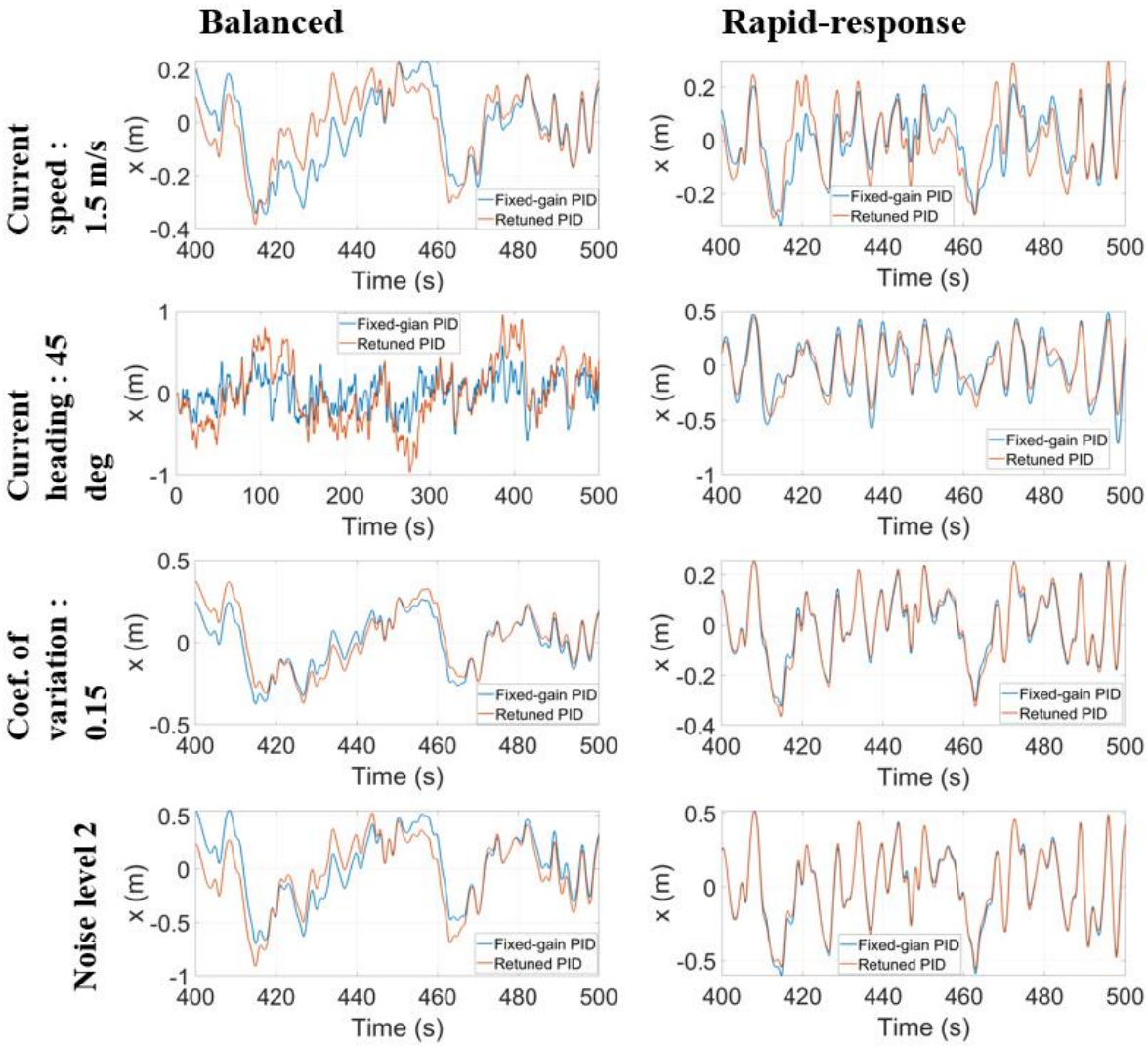

Figure 6-14 Comparison of responses from using fixed gains vs retuned gains, x-position

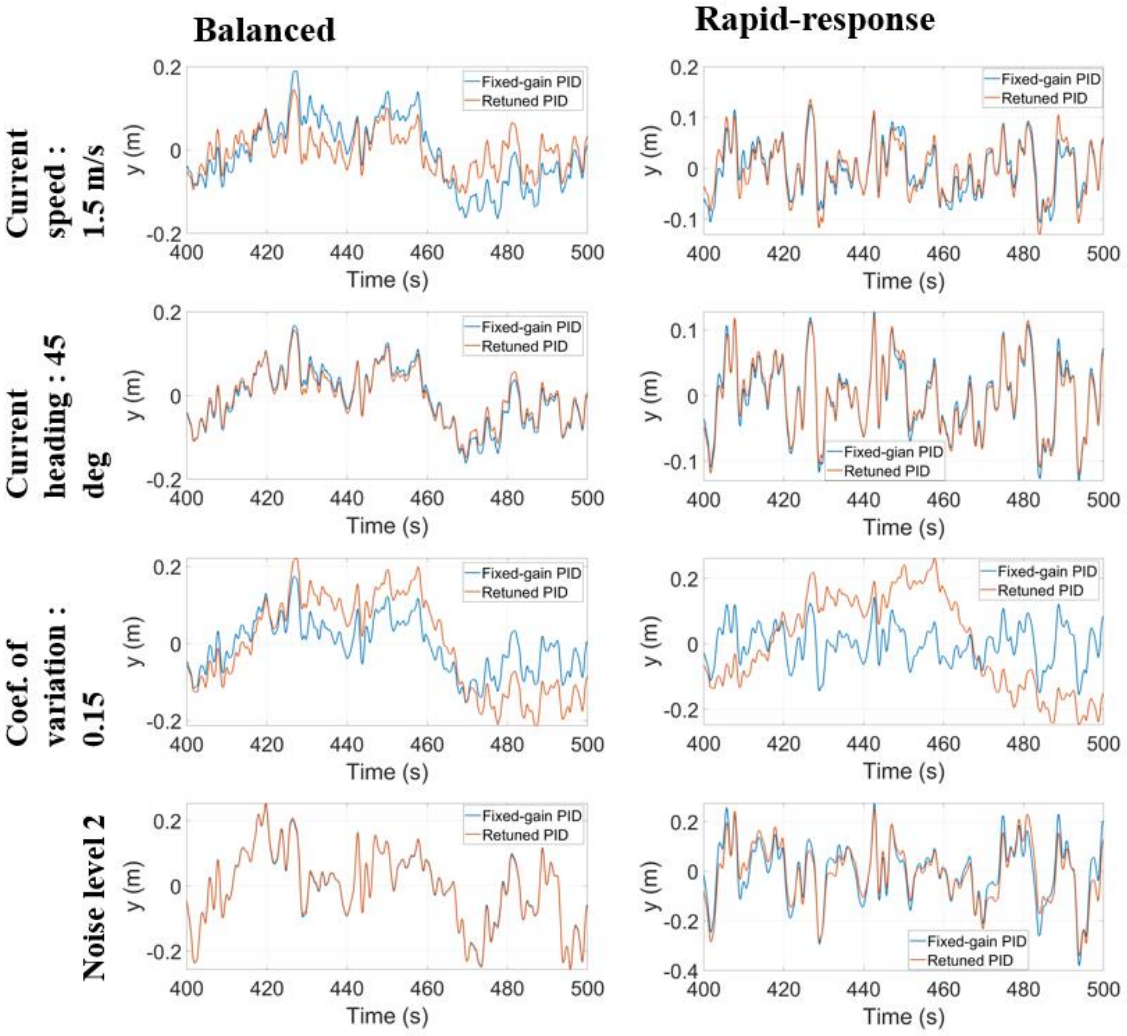

Figure 6-15 Comparison of responses from using fixed gains vs retuned gains, y-position

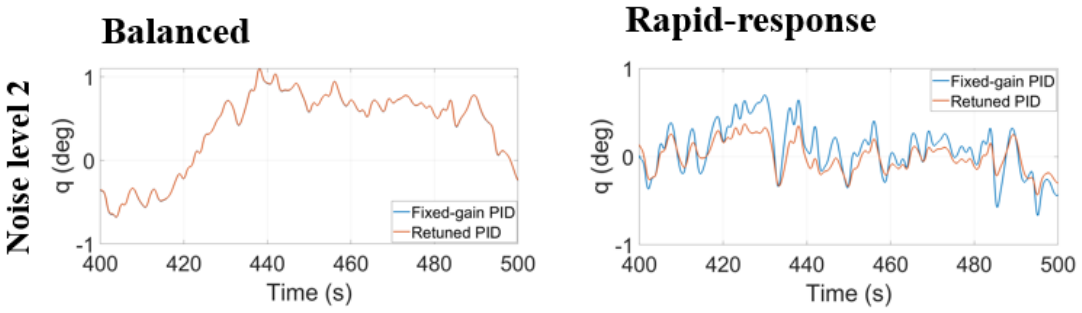

Figure 6-16 Comparison of responses from using fixed gains vs retuned gains, heading

Chapter 7 Conclusion and Further work

8.1. Conclusion

In this thesis, a tuning approach for the robust and optimal dynamic positioning control of BlueROV2 subjected to currents with varying speeds and headings is presented. The results show that the tuning a model solely using step responses from a linearized model might not produce optimal results. Further it is important to verify the system reponses in time domain after tuning. Finally, it is observed that re-tuning the controllers for each simulation case generally leads to better performance. However, it is also shown that the base case controller gains are sufficiently robust and lead to good performances for the other simulation cases.

8.2. Further work

Since a 2D planar dynamic model of BlueROV2 is adopted in this thesis, the most obvious and urgent work to do is to extend the model to a full 3D model. During this process, many assumptions made in this thesis are recommended to be shifted to fit the actual values or properties such as added mass inertia, damping coefficient and the uncoupling among each motion etc.

A proper ROV state observation/estimation system must be developed if the accuracy of simulation is highly required.

In control design part, many other types of controllers or control algorithms are alternative, for example, sliding mode control (SMC) which is considered more optimal than PID control. As for tuning for PID controller, other tuning methods can be tried. Moreover, comparison among different controllers, among different tuning methods can be made.

Concerning on the results and discussion part in this thesis, more cases with different combinations of variables can be run. The relationship between system performance of

step responses and time domain system responses has not been explored yet using the tuning method applied in this thesis.

In the end, a set of immersion tank experiments should be carried out to verify the simulation results if space and equipment available.

Reference

Antonelli, G., et al. 2001. Adaptive control of an autonomous underwater vehicle: experimental results on ODIN, *IEEE Transactions on Control Systems Technology* **9**(5), 756-765

Åström, K. J. and Hägglund, T. 2006. *Advanced PID Control*, NC, Research T. Park:ISA

Bekir E. 2007. I*ntroduction to modern navigation systems[M]*. WORLD SCIENTIFIC, Singapore

Blue Robotics Fathom-X Tether Interface Board Set. https://bluerobotics.com/store/comm-control-power/tether-interface/fathom-x-r1/

Blue Robotics 2017. ArduSub Project. https://www.ardusub.com/

Blue Robotoics. 2021. BlueROV2 Datasheet.

Capocci R., Dooly G., and Omerdic E. et al. 2017. Inspection-Class Remotely Operated Vehicles—A Review, *Journal of Marine Science and Engineering* **5**(1), 13

Christ R.D. amd Wernli R.L. 2014. *The ROV Mannual: a User Guide for Remotely Operated Vehicles (second ed.)*, Elsevier, Oxford, UK

Crowe J., Tan K.K., Lee T.H. et al. 2005. *PID Control: New Identification and Design Methods*, Springer, London, UK

Do K.D. and Pan J. 2006. Robust path-following of underactuated ships: Theory and experiments on a model ship, *Ocean Engineering* **33,** 1354-1372

Dukan, F., et al. 2011. Dynamic positioning system for a small size ROV with experimental results. *OCEAN, 2011 IEEE-Spain*, 1-10

Fernandes D. d A., Sorensen A. J. and Donha D. C. 2013. Trajectory Tracking Motion Control System for Observation Class ROVs, *IFAC Proceedings Volumes* **46**(33), 251-256

Fernandes D. d A., Sorensen A. J. and Pettersen K.Y. et al. 2015. Output feedback motion control system for observation class ROVs based on a high-gain state observer: Theoretical and experimental results, *Control Engineering Practice* **39,** 90-102

Fossen T.I. 2011. *Handbook of Marine Craft Hydrodynamics and Motion Control*, John Wiley & Sons, West Sussex, UK

Fossen T.I. and Johansen T. A. 2006. A survey of control allocation methods for ships and underwater vehicles, *Control and Automation*, MED'06. 14th Mediterranean Conference on, IEEE

Ludvigsen, M., Johnsen, G. Sørensen, A.J., Lågstad, P.A. and Ødegård, Ø. 2014. Scientific Operations Combining ROV and AUV in the Trondheim Fjord, *Marine Technology Society Journal* **48**(2), 59-71

MathWorks 2021. Simulink. https://se.mathworks.com/products/simulink.html

Meier L. Official Pixhawk Website. https://pixhawk.org/

Raspberry Pi Foundation Raspberry Pi 3 Model B. https://www.raspberrypi.org/products/raspberry-pi-3-model-b/

Schjølberg, I. and Utne, I.B. 2015. Towards autonomy in ROV operations, I*FAC-PapersOnLine* **48**(2), 183-188

Sørensen A. J. 2011. A survey of dynamic positioning control systems, *Annual Reviews in Control*, **35**(1), 123-136

Sørensen A.J. 2011. A survey of dynamic positioning control systems, *Annual Reviews in Control* **35**(1), 123-136

Teague J.,Willans J. and Allen M.,Scott T. mad Day J. 2019. Applied marine hyperspectral imaging; Coral Bleaching from a spectral viewpoint. Spectrosc. Eur. **31**, 13–17

Wu, C.J. 2018. 6-DoF Modelling and Control of a Remotely Operated Vehicle, Master Thesis, Flinders University

Yuh, J. 1990. Modeling and control of underwater robotic vehicles, *IEEE Transactions on Systems, man, and Cybernetics* **20**(6), 1475-1483.

Appendix

Tuning for Robust and Optimal Dynamic Positioning Control in BlueROV2

Xu Yang[1], Yihan Xing[1]

[1] Department of Mechanical and Structural Engineering and Materials Science, University of Stavanger, Stavanger, Norway

E-mail:
xu.yang@stud.uis.no
yihan.xing@uis.no

Received xxxxxx
Accepted for publication xxxxxx
Published xxxxxx

Abstract

A tuning approach for the robust and optimal dynamic positioning control of BlueROV2 subjected to currents with varying speeds and headings is presented. A 2D planar dynamic model of BlueROV2 is developed in Matlab/Simulink and used for the study. The surge, sway and yaw motions are controlled by individual PID controllers. An extensive sensitivity study is carried out on a total of nine cases with different current speeds, current headings and measurement noise levels. The results show that the tuning a model solely using step responses from a linearized model might not produce optimal results. Further it is important to verify the system reponses in time domain after tuning. Finally, it is observed that re-tuning the controllers for each simulation case generally leads to better performance. However, it is also shown that the base case controller gains are sufficiently robust and lead to good performances for the other simulation cases.

Keywords: ROV, Simulink modelling, Dynamic positioning, PID control and tuning

1. Introduction

There has been a general increase in interest in the study of underwater vehicles in recent years 0. Underwater vehicles can be classified as remotely operated vehicles (ROVs) 0 and autonomous underwater vehicles (AUVs). These are commonly used in a wide range of underwater missions in many industries such as aquaculture, defence and oil and gas. A ROV is usually controlled by an operator on the ship or on shore via a tether and are used for a wide range of operations from inspection to intervention work. AUVs on the other hand operate independently underwater for longer periods of time and are normally utlised for inspection work. A brief comparison of the important features in ROV and AUV is presented in Table 5.

Table 5 Comparsion between ROV and AUV

Feature	ROV	AUV
Controllability	More controllable; controlled remotely by operators	Without any manual intervention; controlled by a pre-set program
Working range	Limited due to tether length	No limitation
Ability	Multifunctional with different tools	Commonly with single function
Dynamics	Generally fully-actuated	Generally underactuated

Accurate, optimal and robust navigation is crucial for these vehicles to operate effectively underwater. During some operations, such as dynamic positioning 0, path tracking or target following, the ROV would also work like an AUV controlled by a pre-set program. In this paper, the authors will investigate the implementation of dynamic positioning in the BlueROV2 0 as illustrated in Figure 17. BlueROV2 is a popular commercial mini ROV produced by Blue Robotics that is commonly used in scientific research. For example, BlueROV2 has been used as an imaging tool for the

exploration of coral bleaching 错误!未找到引用源。. Although BlueROV2 is a tethered underwater vehicle, it still has the possibility to be easily modified into an autonomous vehicle due to its utilisation of open-source software. This provides a fully-featured open-source solution for ROVs and AUVs allowing the BlueROV2 to work with a wide variety of hardware such as sonar sensors, cameras and inertial navigation system. Autonomous capabilities can be implemented on the BlueROV2 with custom-written code utilising these hardware. For example, Ludvigsen et al. discussed the implemention of computer vision assisted naviation in BlueROV2 0. More details of BlueROV2 are presented in Section 2.

Figure 17 BlueROV2 (base version)

A 2D planar model of the BlueROV2 is developed to study the dynamic positioning problem as illustrated in Figure 18 where the BlueROV2 is subjected to a gaussian current coming in at an aribitary gaussian heading.

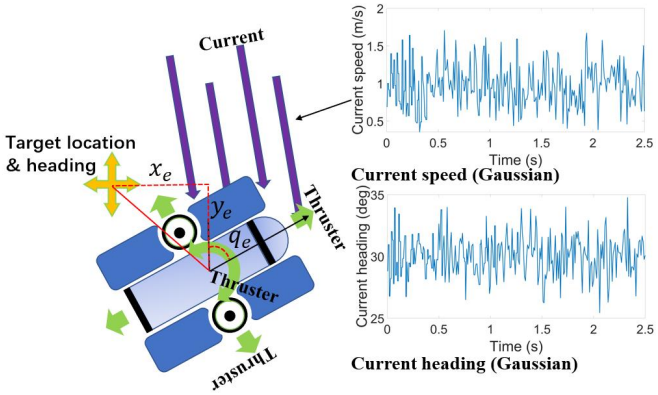

Figure 18 Dynamic positioning of BlueROV2 subjected to a current coming at an arbitrary heading

The dynamic positioning is controlled using proportional-integral-derviative (PID) control 0. The PID tuner and autotuner tools from Simulink 0 are used for the tuning of the controller gains. More details of the model and the tuners are provided in Section 3. Even though a 2D planar problem using PID control is studied in this paper, the model can be easily extended to be a full 3D model and to use other more advanced control methods.

2. Description of BlueROV2

The BlueROV2 used in this paper and previously presented in Figure 17 is the base version offered by Blue Robotics. It is a mini observation class ROV that can operate up to 100 m. It is equipped with four horizontal and two vertical T200 thrusters which allows propulsion in 6 independent DOFs. The thrustor configuration is presented in Figure 19.

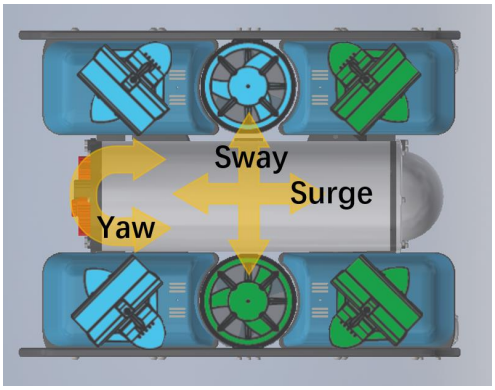

Figure 19 Thruster configuration of BlueROV2 from top view. Green and blue represent counter-clockwise and clockwise propellers, respectively.

BlueROV2 is driven by the open-source Ardusub software 0 running on a open-source Pixhawk autopilot system 0. The PixHawk autopilot is a powerful open-source hardware platform that has an on-board inertia measurement unit and multiple I/O ports and has been adapted for use in a wide variety of drones (air/land/sea). The Raspberry Pi 3 0 is used as a companion computer to provide HD video streaming to the surface workstation via the tether and Fathom X interface 0. The main BlueROV2 parameters are presented in Table 6.

Table 6 Main BlueROV2 parameters

Parameters	Symbol	Value	Unit
Length	L	0.457	m
Width	W	0.338	m
Height	H	0.254	m
Mass	m	10.565	kg
Yaw moment	I_{zz}	0.201	kg · m
Surge added mass	I_{Ax}	10.565	kg
Sway added mass	I_{Ay}	10.565	kg
Yaw added mass	I_{An}	0.201	kg · m
Quadratic damping coefficient	C_D	0.5	-
Surge cross section area	A_x	0.048	m^2
Sway cross section area	A_y	0.10	m^2
Yaw cross section area	A_n	0.07	m^5

3. Theory

As mentioned, this paper will focus on 2D planar dynamics, i.e., only x-y plane motions are considered and there is no heave, roll and pitch motions. In addition, the following assumptions are made:

- The BlueROV2 is assumed to be hydrodynamically symmetrical, i.e., there are no hydrodynamic coupling terms.
- The BlueROV2 is assumed to operate far away from the wave-affected zone, i.e., the load-effects of waves are negligible and only currents will be considered.

3.1 Equations of motion

The equations of motions for a ROV can be described by the Newton-Euler equation as presented by Fossen 0:

$M\dot{v} + C(v)v + D(v)v + g(\eta) = \tau$	**Eq. (2)**

Where M is the mass matrix, $C(v)$ is the Coriolis matrix, $D(v)$ is the damping matrix, $g(\eta)$ is the gravitational forces and moments, v is the velocity and τ is the external driving forces.

For a 2D x-y planar dynamic problem solved in a global earth frame at a fixed latitude, $C(v)$ and $g(\eta)$ are zero and Eq. (1) can be simplified and expanded to:

$\begin{bmatrix} m+I_{Ax} & 0 & 0 \\ 0 & m+I_{Ay} & 0 \\ 0 & 0 & I_{zz}+I_{An} \end{bmatrix} \begin{bmatrix} \dot{u} \\ \dot{v} \\ \dot{w} \end{bmatrix} + \frac{1}{2}\rho C_D A \begin{bmatrix} \lvert u\rvert \\ \lvert v\rvert \\ \lvert w\rvert \end{bmatrix} \cdot \begin{bmatrix} u \\ v \\ w \end{bmatrix} = \begin{bmatrix} X \\ Y \\ T \end{bmatrix}$	**Eq. (3)**

Where $[u \quad v \quad w]^T$ are the velocities in surge, sway, yaw respectively, $[\dot{u} \quad \dot{v} \quad \dot{w}]^T$ are the accelerations in surge, sway, yaw respectively and $[X \quad Y \quad T]^T$ are forces and moment in surge, sway, yaw. $[I_{Ax} \quad I_{Ay} \quad I_{An}]$ are added mass components, ρ is the density of water, C_D is the drag coefficient and A is the cross section area for drag. Added mass on a rigid body is a virtual mass caused by the fluid around. In this study, added mass $[I_{Ax} \quad I_{Ay} \quad I_{An}]$ are asummed to be the same as the mass and inertia moment of BlueROV2 as listed in Table 6.

Based on the assumption of hydrodynamic symmetry, the coupled terms have all not been considered. Correspondingly, the drag force can be regarded to be proportional to the square of the relative velocity between current and act in the opposite direction to the ROV's motion. Given the above, drag forces in surge, sway and yaw can be expressed respectively as:

$X_D = -\frac{1}{2}\rho C_D A_x \lvert u\rvert u$	**Eq. (4)**
$Y_D = -\frac{1}{2}\rho C_D A_y \lvert v\rvert v$	**Eq. (5)**
$\psi_D = -\frac{1}{2}\rho C_D A_n \lvert w\rvert w$	**Eq. (6)**

The drag coefficients for three DOFs are all assumed to be 0.5 in this study. The cross section areas for each direction are listed in Table 6.

3.2 Proportional-integral-derivative control

PID control is commonly adopted in unmanned underwater vehicles and marine operation field 0. Two types of PID controllers are considered in this paper. One is a general PID controller that uses fixed controller gain values while the other one is an auto-tuned PID controller that is able to adapt the controller gains automatically for different scenarios.

Using the PID controller, the open-loop BlueROV2 control system can transformed to a closed-loop control as shown in Figure 30. There are three PID controllers used, one for each individual directions, i.e., surge, sway and yaw.

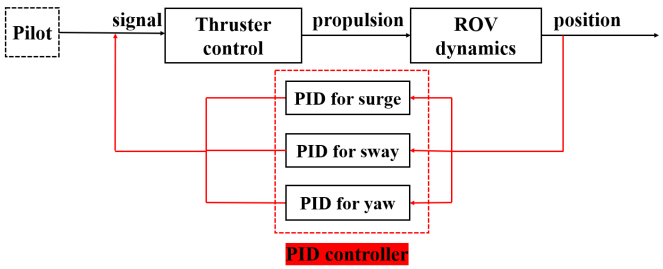

Figure 30 From open-loop control sysem to closed-loop control system with PID controller

The input for a PID controller is the error $e(t)$ between the measured process variable and the desired setpoint. The output $u(t)$ is produced with a correction multiplied by a proportional gain (K_P), integral of the correction multiplied by an integral gain (K_I) and derivative of the correction multiplied by a derivative gain (K_D). The overall function of PID controller is given below:

$u(t) = K_p e(t) + K_i \int_0^t e(t)\,dt + K_d \frac{de(t)}{dt}$	**Eq. (7)**

In this study, $e(t)$ is the errors $[x_e \quad y_e \quad q_e]$ between the measured position of BlueROV2 $[x_m \quad y_m \quad q_m]$ and coordinate of the desired point $[x_t \quad y_t \quad q_t]$. The output is the thruster forces signal $[F_x' \quad F_y' \quad T_q']$ used to control the BlueROV2 to approach the target. Since the input and output in this control system are both 3-dimensional, and each two of three components are uncoupled. As mentioned above, the PID controller used in is decentralized into 3 sub-PID controller for x_e & F_x', y_e & F_y' and q_e & T_q', respectively. Tuning of this ROV motion control system involves the controller gains of individual PID controllers in surge, sway and yaw, i.e., their corrsponding K_p, K_i and K_d values. As mentioned, two tuning methods are investigated in this paper. The first tuning method involves using a single set of K_p, K_i and K_d values for the whole system running process after proper tuning. The second tuning method uses K_p, K_i and K_d values that are retuned for each load case. In this way the

control gains can be in theory adapted to different types of envoironmental loads and noise level.

3.3 Tuning and desired system performance

The tuning tool used in this study is the Matlab PID tuner which works by principle of 0. The PID tuner uses a system model linearised at an operating point for tuning. By changing the Bandwidth and Phase margin setting in frequency domain, the tuner will derive the corresponding controller gains automatically and also plot out the system impulse response. In this study, rise time (T_{rise}), setting time ($T_{setting}$), percentage overshoot (PO) and gain margin (γ) are used performance indicators. These are briefly discussed in the following and presented in **Figure 21**.

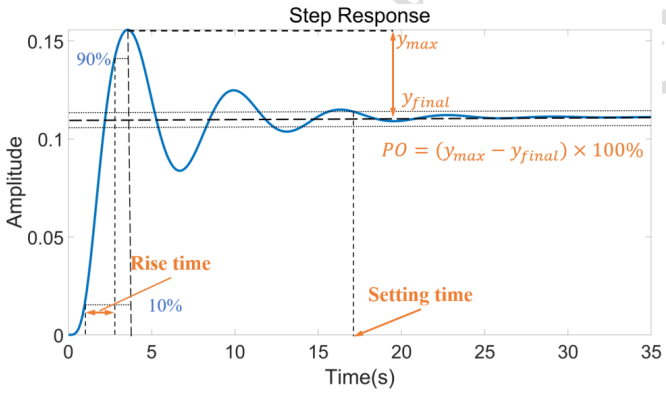

Figure 21 Rise time, setting time and overshoot

Rise time is defined as the time period for the system to rise from 10% to 90% of the steady state value. Rise time represents the respond speed of the system. It is desired to have a quick response, i.e., below 3 seconds for the BlueROV2. Setting time of a system is the time it takes for the error $e(t)$ to fall below 2% of the peak value of $e(t)$. A setting time reflects the ability of the system to stabilised. It is desired that the settling time of the BlueROV2 be less than 50 seconds. Percentage overshoot in a control system is the percentage of the maximum peak value of the response exceeding the final, steady-state value as expressed in Eq. (8). A larger overshoot represents more potential oscillation or less stability. It is desired to have an overshoot below 50% in this study. The gain margin is the difference between 0 dB and the gain at the phase-cross-over frequency which is at the phase equals to -180 degree. A larger gain margin means a more stable system. When the gain margin becomes negative, the system is unstable. Gain margins in the interval of $[5, 30]$ dB is desired for the BlueROV2.

$PO = (y_{max} - y_{final}) \times 100\%$	**Eq. (8)**

The base case in this paper has the following two sets of tuning objectives:

- Balanced - rise time < 1.5 s, setting time < 30 s, percentage overshoot < 30 % and gain margin > 5 dB.
- Rapid-response - rise time < 1 s, setting time < 10 s.

4. Simulink implementation

The Simulink implementation is illustrated in Figure 28.

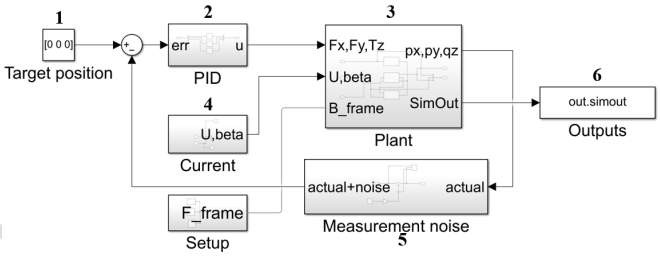

Figure 28 Simulink model diagram

The model consists of the following main blocks as labelled in Figure 28:

- Block 1: Provides the coordinates of the set location (x_{set},y_{set},z_{set}).
- Block 2: Contains the PID controllers. Each individual variable has an independent PID controller, i.e., a de-coupled PID control method is used.
- Block 3: Contains the plant model which considers the 2D planar dynamics of the BlueROV2.
- Block 4: Provides the gaussian current speeds and directions, and the global model set-up parameters.
- Block 5: Adds measurement noise into the ROV displacements measured from the plant model (Block 4).
- Block 6: Stores the simulation outputs.

4.1 Plant model

The plant model (Block 3 in **Figure 28**) is presented in more details in this sub-section. A zoom view into the plant model is presented in **Figure 23**.

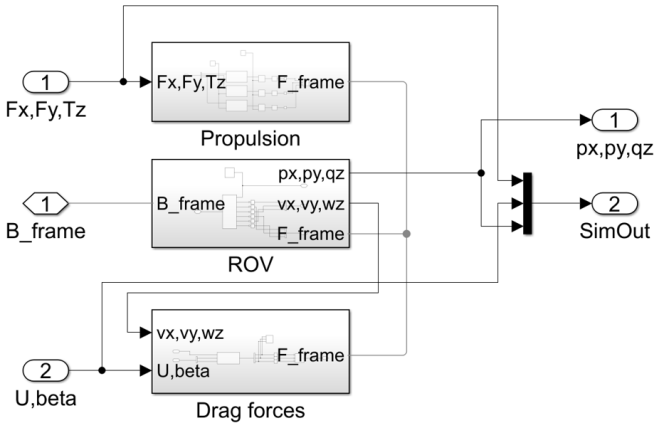

Figure 23 Plant model diagram

The plant model consists of three main blocks:

- Propulsion: This block models the propulsion forces. The block takes in the commanded forces and torque (F_x, F_y and T_z) as inputs and applies them to the ROV block. To remove high frequency noise, a low pass filter with cut-off frequency of 1 Hz is also applied on the commanded signals before they are used as forces and torque. The forward and lateral thurst forces are saturated to [-88.3 ,88.3] N and the yaw moment is saturated to [-17.5 ,17.5] N·m in accordance with the physical limitations of the T200 thrusters.
- ROV: This block contains a 2D planar rigid body with 3 degrees of freedom (x, y and w). Simulink will solve the equation of motion in accordance with Eq. (3) based on the forces and torque applied on the rigid body.
- Drag forces: This block calculates the drag forces and torque based on the current speed and ROV's velocities in accordance with Eq. (4), Eq. (5) and Eq. (6) and then applies them to the ROV block.

5. Case studies

To explore the effect of tuning, several cases with different current speed, heading, coefficient of variation (COV) and measurement noise levels presented in Table 6-1 are considered.

Table 7 Simulation cases

Case name	Current speed	Current heading	COV	Control type	Noise
1-30-0.1-fx-lv1	1 m/s	30 deg	0.1	fixed	Level 1
1.5-30-0.1-fx-lv1	1.5 m/s	30 deg	0.1	fixed	Level 1
1-45-0.1-fx-lv1	1 m/s	45 deg	0.1	fixed	Level 1
1-30-0.15-fx-lv1	1 m/s	30 deg	0.15	fixed	Level 1
1-30-0.1-fx-lv2	1 m/s	30 deg	0.1	fixed	Level 2
1.5-30-0.1-tn-lv1	1.5 m/s	30 deg	0.1	tuned	Level 1
1-45-0.1-tn-lv1	1 m/s	45 deg	0.1	tuned	Level 1
1-30-0.15-tn-lv1	1 m/s	30 deg	0.15	tuned	Level 1
1-30-0.1-tn-lv2	1 m/s	30 deg	0.1	tuned	Level 2

The first case, i.e., 1-30-0.1-fx-lv1 is the base case. 'fixed' mean that the parameters K_p, K_i, K_d and filter coefficient N are fixed as the same as those tuned in the base case. 'tuned' means K_p, K_i, K_d and N are retuned to adapt to the current case. The objective in the retuning is to readjust the bandwidth and phase margin back to the same values as in the base case. Level 1 means that the gain for noise in surge direction = 0.001, gain for noise in sway direction = 0.001 and gain for noise in yaw motion = 0.00001. Level 2 means that the gain for noise in surge direction = 0.002, gain for noise in sway direction = 0.002 and gain for noise in yaw motion = 0.00002.

6. Results and discussions

6.1 Base Case gains

The controller gains for the Base Case (1-30-0.1-fx-lv1) are presented in Table 6-2 and Table 6-3 when balanced tuning and rapid-response tuning approaches are used, respectively. The tuning objectives were previously discussed in Section 3.3.

Table 8 PID gains for Base Case with balanced tuning

	K_p	K_i	K_d	N
Surge	3.4619	0.0275	21.157	109.48
Sway	10.901	0.7667	20.531	100.06
Yaw	0.0084	0.000043	0.3632	100.52

Table 9 PID gains for Base Case with rapid-response tuning

	K_p	K_i	K_d	N
Surge	14.936	0.1468	21.752	130.23
Sway	26.426	7.6454	22.681	118.54
Yaw	0.1260	0.00125	0.4818	135.08

A comparison of the time series of the x-position, y-position and heading angle when balanced and rapid-response tuning approaches are used is presented in Figure 6-1 Times series of x-position, Base case, 1-30-0.1-fx-lv1, Balanced vs Rapid-response tuning approach.

. As observed, the rapid-response approach leads to a faster system response; the orange line tends to lead the blue line in Figure 6-1 Times series of x-position, Base case, 1-30-0.1-fx-lv1, Balanced vs Rapid-response tuning approach.

. This effect is particularly pronounced in the heading angle response.

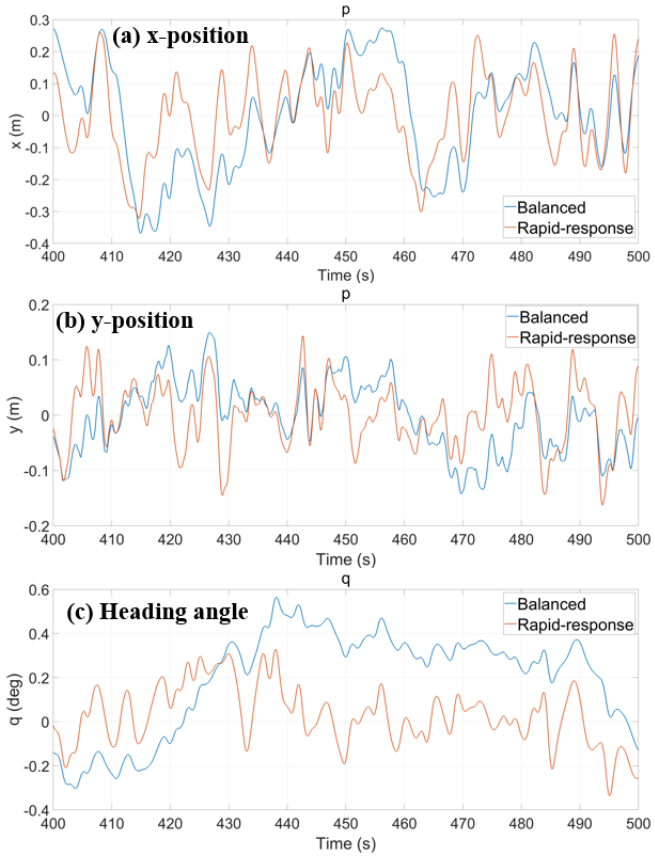

Figure 24 Times series of x-position, Base case, 1-30-0.1-fx-lv1, Balanced vs Rapid-response tuning approach.

6.2 Sensitivity study performed on Base Case

A sensitivity study is performed on the base case (1-30-0.1-fx-lv1) to explore the relationship between controller gains and performance in term of rise time, settling time, overshoot and gain margin. The study is performed on a model linearised at t = 450 s. The surge (x-dir) component is presented. The results are presented in Figure 25, Figure 26, Figure 27 and Figure 28, for rise time, settling time, overshoot and gain margin, respectively.

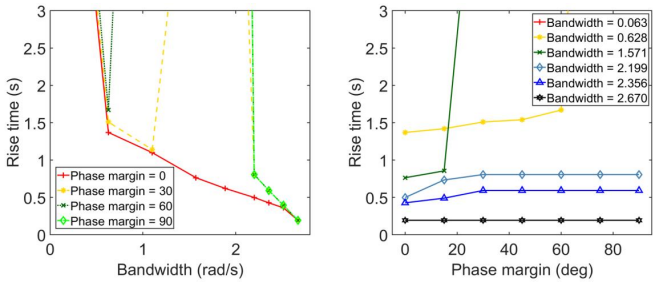

Figure 25 Base Case (1-30-0.1-fx-lv1), Surge (x-dir), Rise Time vs Bandwith and Phase Margin

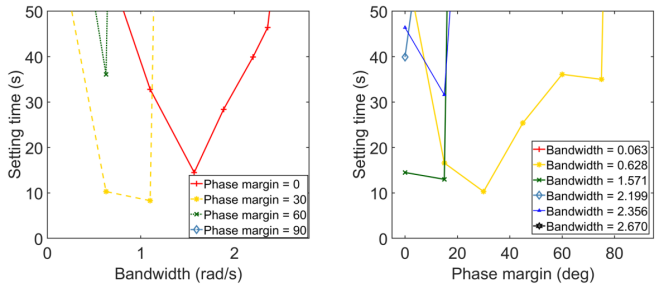

Figure 26 Base Case (1-30-0.1-fx-lv1), Surge (x-dir), Settling Time vs Bandwith and Phase Margin

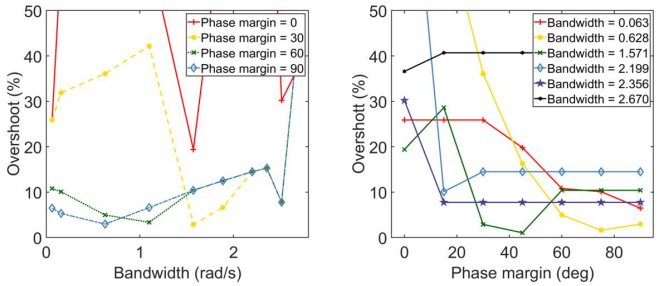

Figure 27 Base Case (1-30-0.1-fx-lv1), Surge (x-dir), Overshoot vs Bandwith and Phase Margin

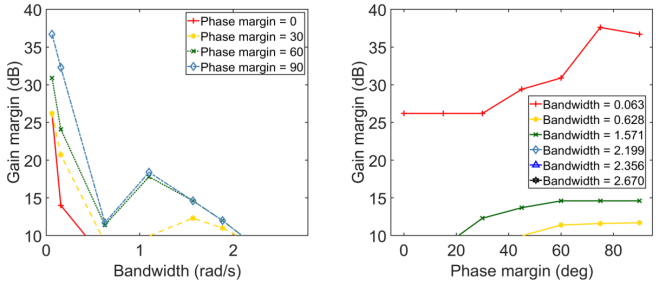

Figure 28 Base Case (1-30-0.1-fx-lv1), Surge (x-dir), Gain Margin vs Bandwith and Phase Margin

The following observations are made:

- Rise time decreases rapidly with increasing bandwidth, but is not affected by changes in phase margin.
- Settling time has a convave relationship (decreases then increases) with increasing bandwidth and phase margin.

- Overshoot is not affected by changes in bandwidth but decreases with increasing phase margin.
- Gain margin decreases with increasing values of bandwidth increasing but is not affected by changes in phase margin.

The above observations provide guidance for the subsequent controller tuning process that is performed in this paper.

6.3 Parametric correlation analysis

A parametric correlation analysis is performed to quantify the relationship between controller gains and performance variables. From the sensivitity study performed in Section 6.1, it is obvious that the relationships between these are nonlinear. Therefore, determination matrix which quantifies quadratic correlations is computed. The coefficient of determination, r^2 that relates variables x and y is expressed as:

$$r^2 = \frac{\sum(y_i - \bar{y})^2 - \frac{n-1}{n-2}(y_i - Y_i)^2}{\sum(y_i - \bar{y})^2} \qquad \textbf{Eq. (9)}$$

Where n is the total number of samples and $Y_i = ax_i^2 + bx_i + c$. The coefficient of determination has a value of 0 to 1. A value of 0 means no correlation, while a value of 1 means perfect correlation. The determination matrix is presented in Figure 29.

	Bandwidth	Phase margin	Rise time	Settling time	Overshoot	Gain margin	Kp	Ki	Kd
Bandwidth	1.00	0.00	0.22	0.01	0.01	0.66	0.16	0.10	0.16
Phase margin	0.00	1.00	0.22	0.20	0.48	0.10	0.47	0.42	0.00
Rise time	0.44	0.21	1.00	0.28	0.15	0.65	0.16	0.08	0.37
Settling time	0.05	0.34	0.35	1.00	0.27	0.07	0.24	0.27	0.13
Overshoot	0.00	0.40	0.17	0.27	1.00	0.14	0.23	0.23	0.03
Gain margin	0.64	0.10	0.34	0.08	0.19	1.00	0.21	0.16	0.53
Kp	0.14	0.39	0.14	0.07	0.22	0.28	1.00	0.63	0.57
Ki	0.03	0.33	0.07	0.08	0.25	0.13	0.71	1.00	0.00
Kd	0.97	0.01	0.17	0.01	0.04	0.51	0.10	0.04	1.00

Figure 29 Determination Matrix

The following observations are made:

- Rise time has an inverse quadratic coefficient of determination of 0.44 which means it has a somewhat quadratic relationship with bandwidth.
- The quadratic coefficients of determination between setting time and phase margin are 0.28 and 0.34 (inverse). This means a slight correlation.
- Percentage overshoot has quadratic coefficients of determination of 0.48 and 0.40 (inverse) with phase margin which means they are fairly correlated.
- The quadratic coefficients of determination between gain margin and bandwidth are 0.66 and 0.64 (inverse) which indicates a relatively strong correlaton.

The observations are summarized in Table 6-4. '+' indicates improved performance, '–' indicates impaired performance and '0' indicates no clear trend.

Table 10 Summary of observations from determination matrix

Performance variable	Bandwidth	Phase margin
T_{rise}	++	0
$T_{settling}$	+-	+-
PO	0	++
γ	-	0

6.4 Different simulation cases

The other different simulation cases presented in Table 6-1 are studied in this sub-section using controller gains derived from both balanced and rapid-response approaches.

6.4.1 Step responses using Base Case gains The system step responses when base case gains are used are presented in Figure 30 and Figure 31 for the balanced and rapid-response tuning approaches, respectively.

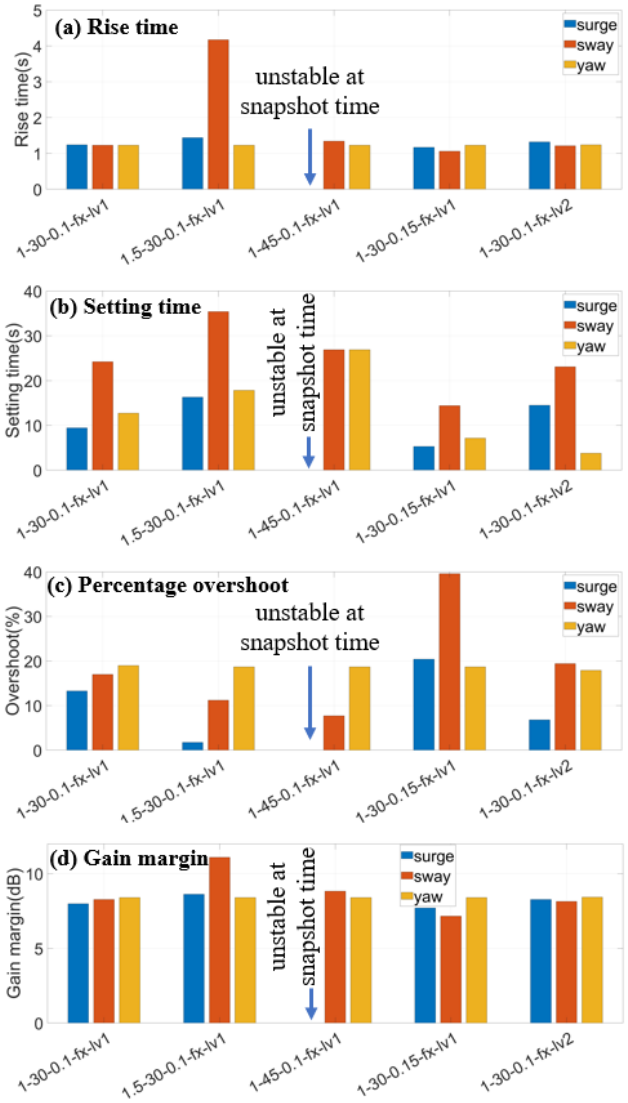

Figure 30 Balanced tuning approach, Step responses for different simulation cases, (a) Rise time, (b) Setting time, (c) Percentage overshoot and (d) Gain margin

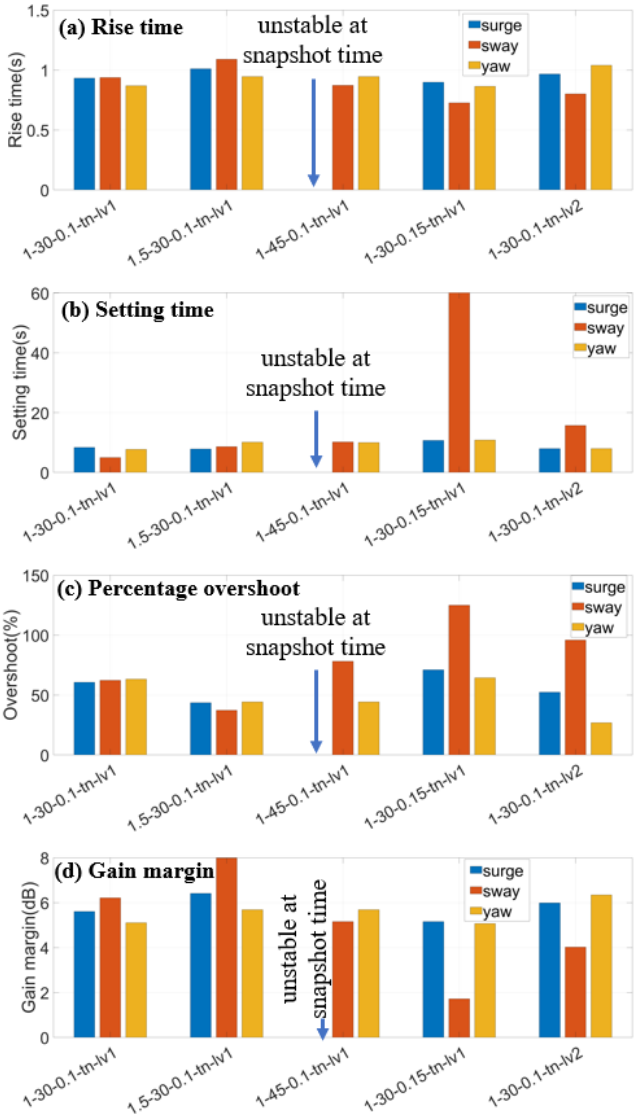

Figure 31 Rapid-response tuning approach, Step responses for different simulation cases, (a) Rise time, (b) Setting time, (c) Percentage overshoot and (d) Gain margin

In general, it is observed that the step responses are in general similar for the different cases except for the following cases:

- Surge component in 1-45-0.1-fx-lv1 and 1-45-0.1-tn-lv1: The system is unstable under a current heading of 45 degree.
- Sway component in 1.5-30-0.1-fx-lv1: The rise time increases when the balanced tuning approach is used. The settling time becomes are large as 60 seconds when the rapid-response tuning approach is used.

To explore how these exceptions will affect the BlueROV2's performance, the time series of responses will be shown and discussed in the following sub-section.

6.4.2 Time series of responses

The time series of the corresponding responses of the cases presented in Figure 30 and Figure 31 are presented in **Figure 32**, **Figure 33** and **Figure 34** for the x-position, y-position and heading, respectively. In general, actual time domain responses show larger differences between the different simulation cases compared to that observed from the step responses presented in Section 6.4.1. This means that it is important not to purely and over rely on the step responses when tuning is performed. It is important to always test the system out in time domain and observe the actual time domain responses. It is also observed that the rapid-response tuning approach produces a somewhat poorer performance compared to the balanced tuning approach.

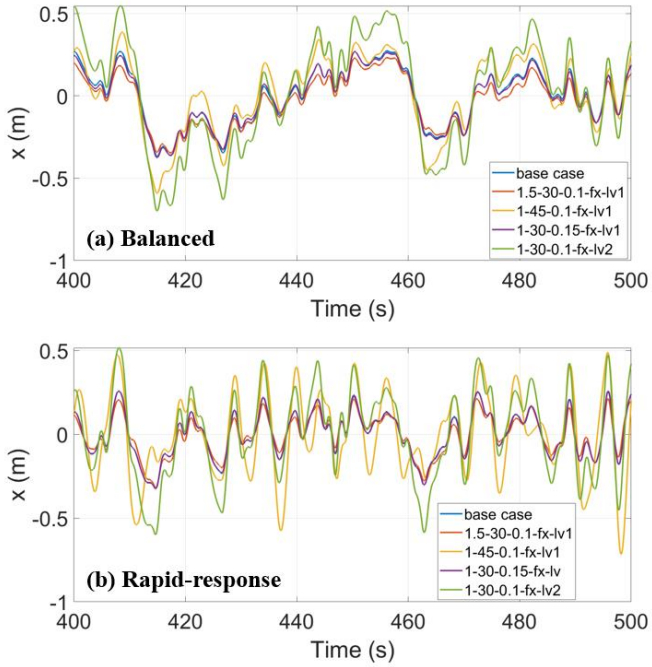

Figure 32 x-position for different simulation cases, (a) Balanced tuning, (b) Rapid-response tuning

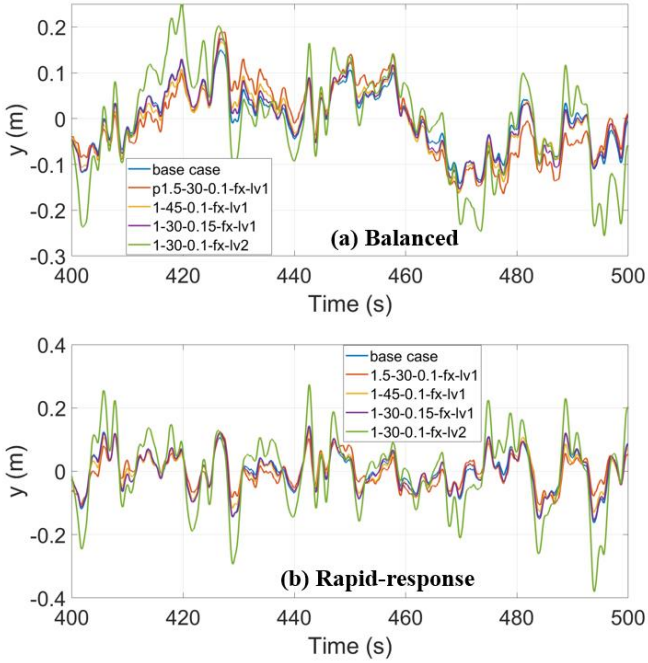

Figure 33 y-position for different simulation cases, (a) Balanced tuning, (b) Rapid-response tuning

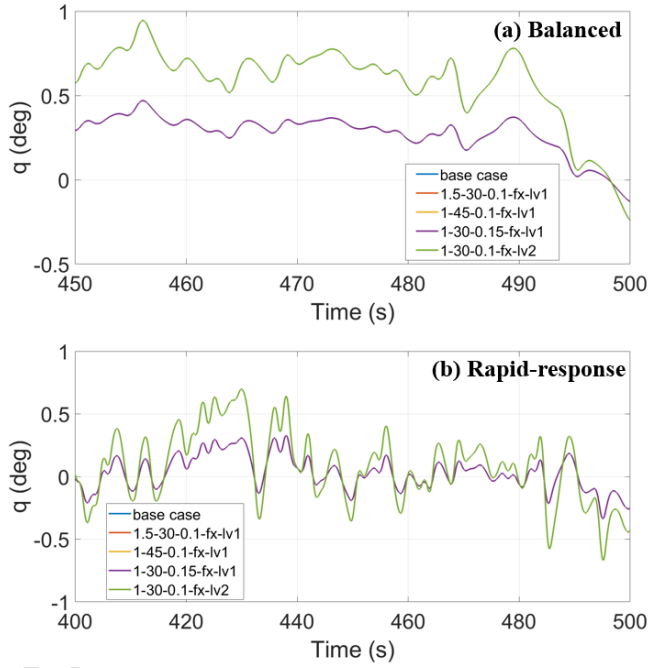

Figure 34 Heading for different simulation cases, (a) Balanced tuning, (b) Rapid-response tuning

6.4.3 Effect of re-tuning

In this section, improvements will be attempted on the time domain performances presented in Section 6.4.2 by performing re-turning for each simulation case. The time domain responses are presented in Figure 35, Figure 36 and Figure 37, respectively for x-postion, y-position and heading.

In general, it is observed that re-tuning the PID controllers leads to better performances.

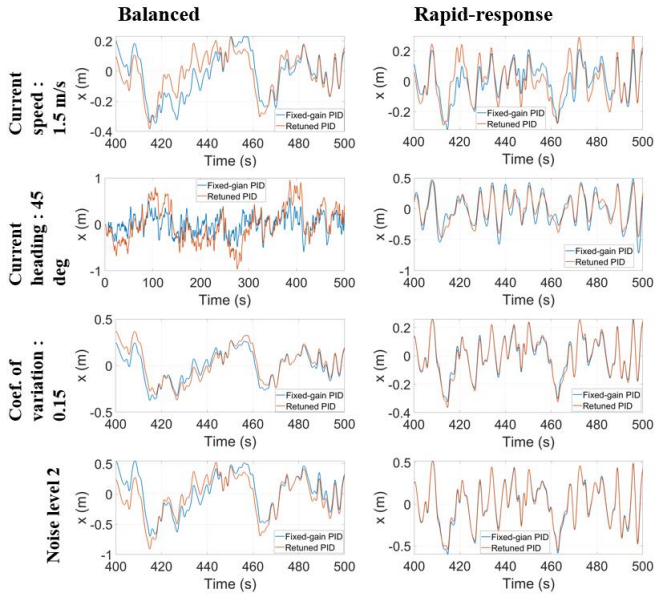

Figure 35 Comparison of responses from using fixed gains vs retuned gains, x-position

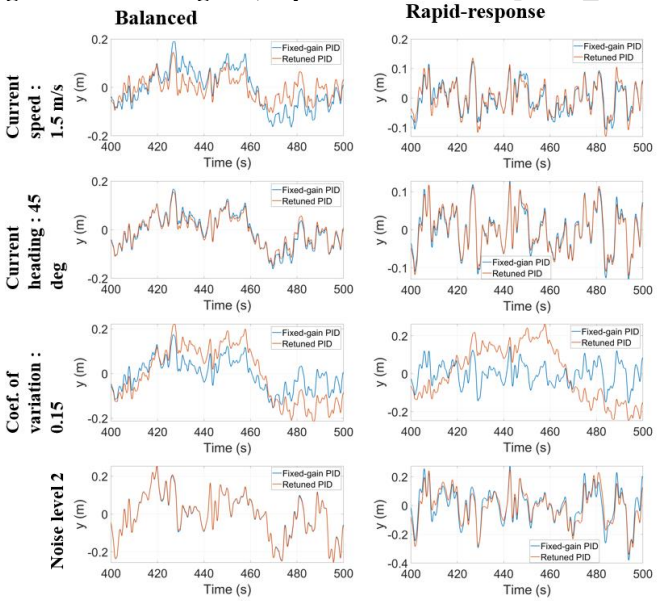

Figure 36 Comparison of responses from using fixed gains vs retuned gains, y-position

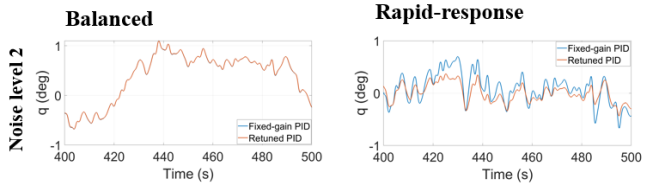

Figure 37 Comparison of responses from using fixed gains vs retuned gains, heading

7. Conclusions

In this paper, a tuning approach for the robust and optimal dynamic positioning control of BlueROV2 subjected to currents with varying speeds and headings is presented. The results show that the tuning a model solely using step responses from a linearized model might not produce optimal results. Further it is important to verify the system reponses in time domain after tuning. Finally, it is observed that re-tuning the controllers for each simulation case generally leads to better performance. However, it is also shown that the base case controller gains are sufficiently robust and lead to good performances for the other simulation cases.

References

Wu, C.J. 2018. 6-DoF Modelling and Control of a Remotely Operated Vehicle, Master Thesis, Flinders University

Christ R.D. amd Wernli R.L. 2014. *The ROV Mannual: a User Guide for Remotely Operated Vehicles (second ed.)*, Elsevier, Oxford, UK

Sørensen A.J. 2011. A survey of dynamic positioning control systems, *Annual Reviews in Control* **35**(1), 123-136

Blue Robotoics. 2021. BlueROV2 Datasheet.

Teague J.,Willans J. and Allen M.,Scott T. mad Day J. 2019. Applied marine hyperspectral imaging; Coral Bleaching from a spectral viewpoint. Spectrosc. Eur. **31**, 13–17

Ludvigsen, M., Johnsen, G. Sørensen, A.J., Lågstad, P.A. and Ødegård, Ø. 2014. Scientific Operations Combining ROV and AUV in the Trondheim Fjord, *Marine Technology Society Journal* **48**(2), 59-71

Crowe J., Tan K.K., Lee T.H. et al. 2005. *PID Control: New Identification and Design Methods*, Springer, London, UK

MathWorks 2021. Simulink. https://se.mathworks.com/products/simulink.html

Blue Robotics 2017. ArduSub Project. https://www.ardusub.com/

Meier L. Official Pixhawk Website. https://pixhawk.org/

Raspberry Pi Foundation Raspberry Pi 3 Model B. https://www.raspberrypi.org/products/raspberry-pi-3-model-b/

Blue Robotics Fathom-X Tether Interface Board Set. https://bluerobotics.com/store/comm-control-power/tether-interface/fathom-x-r1/

Fossen T.I. 2011. *Handbook of Marine Craft Hydrodynamics and Motion Control*, John Wiley & Sons, West Sussex, UK

Schjølberg, I. and Utne, I.B. 2015. Towards autonomy in ROV operations, I*FAC-PapersOnLine* **48**(2), 183-188

Åström, K. J. and Hägglund, T. 2006. *Adv*

anced PID Control, NC, Research T. Park:ISA